TAMPEREEN TEKNILLINEN YLIOPISTO
TAMPERE UNIVERSITY OF TECHNOLOGY

MARTTA HÄKLI

MATURATION OF HUMAN INDUCED PLURIPOTENT STEM CELL-DERIVED CARDIOMYOCYTES GROWN ON POLYETHYLENE TEREPHTHALATE TEXTILES

Master of Science Thesis

Examiners: professor Minna Kellomäki, senior researcher Mari Pekkanen-Mattila
Examiners and topic approved by the Faculty Council of the Faculty of Natural Sciences
1. November 2017

ABSTRACT

MARTTA HÄKLI: Maturation of human induced pluripotent stem cell-derived cardiomyocytes grown on polyethylene terephthalate textiles
Tampere University of Technology
Master of Science Thesis, 70 pages
March 2018
Master's Degree Programme in Biotechnology
Major: Tissue engineering
Examiners: Professor Minna Kellomäki, Senior researcher Mari Pekkanen-Mattila

Keywords: cardiomyocyte, human induced pluripotent stem cell, maturation, gene expression, calcium cycling, polyethylene terephthalate, textile

Human cardiomyocytes (CMs) have been difficult to obtain due to invasive heart biopsies and poor long-term survival of the cells, limiting their utilization in research of cardiac diseases. Human induced pluripotent stem cells (hiPSCs) provide an unlimited source of human CMs that can be utilized in developing patient-specific disease models and tissue engineering applications, and in drug screening. However, when hiPSC-derived CMs (hiPSC-CMs) are cultured in *in vitro* conditions, they are developmentally immature compared to adult human CMs, which is why the collected data cannot be directly related to the actual disease. Many methods have been developed to improve the maturation state of the hiPSC-CMs, including different kinds of topographical and chemical cues, but none has succeeded in producing CMs comparable to the adult human CMs. The aim of this study was to determine would culturing hiPSC-CMs on polyethylene terephthalate (PET) textiles affect molecular and functional maturity state of the cells in addition to structural maturation.

hiPSC were differentiated into CMs using small molecule differentiation and the resulted CMs were sorted via magnetic-activated cell sorting (MACS) and plated onto gelatin-coated PET textiles for 11-12 days. Control cells were cultured on gelatin-coated coverslips. Molecular maturation was evaluated by comparing the relative expression of cardiac type troponin T (TNNT2) of target and control cells via qPCR. Functional maturation was evaluated by comparing calcium handling properties of the target and control cells via calcium imaging. Structural properties of the target and control cells were compared via immunostaining and fluorescence imaging. The cell shape, sarcomere length and orientation were analyzed from the images with CytoSpectre software.

Culturing hiPSC-CMs on PET textiles seemed to induce molecular, functional and structural maturation of the cells. TNNT2 expression increased 3.35-fold in hiPSC-CMs grown on PET textiles compared to control. hiPSC-CMs grown on PET textiles exhibited less abnormalities in calcium kinetics, and had faster removal of cytosolic calcium and increased beating frequency. Also, cell shape and sarcomere orientation were improved. On the other hand, release of calcium into the cytosol was slower in hiPSC-CMs grown on PET textiles, and sarcomere length of the cells was not affected and was lower than that of observed in adult human CMs.

TIIVISTELMÄ

MARTTA HÄKLI: Polyetyleenitereftalaattitekstiileillä kasvatettujen ihmisen uudelleenohjelmoiduista kantasoluista erilaistettujen sydänlihassolujen maturaatio
Tampereen teknillinen yliopisto
Diplomityö, 70 sivua
Maaliskuu 2018
Biotekniikan diplomi-insinöörin tutkinto-ohjelma
Pääaine: Kudosteknologia
Tarkastaja: professori Minna Kellomäki, erikoistutkija Mari Pekkanen-Mattila

Avainsanat: sydänlihassolu, ihmisen uudelleenohjelmoitu kantasolu, maturaatio, geenieksprессio, kalsiumkierrätys, polyetyleenitereftalaatti, tekstiili

Aikuisen sydänlihassoluja (CMs) on vaikea kerätä, eivätkä ne kestä pitkiä viljelyaikoja. Tämä on rajoittanut niiden käyttöä sydänsairauksien tutkimuksessa. Ihmisen uudelleenohjelmoitavia kantasoluja (hiPSCs) voidaan erilaistaa sydänlihassoluiksi, mikä on mahdollistanut ihmisen sydänlihassolujen käytön henkilökohtaisessa tauti-mallinnuksessa, lääketutkimuksessa ja kudosteknologian sovelluksissa. Ihmisen uudelleenohjelmoitavista kantasoluista erilaistetut sydänlihassolut (hiPSC-CMs) ovat kuitenkin *in vitro* -olosuhteissa kasvatettuina epäkypsiä verrattuna aikuisen sydän-lihassoluihin, mikä vaikeuttaa niistä saatavan tiedon hyödyntämistä tautimallinnuksessa. Näiden solujen ominaisuuksien parantamiseksi on kehitetty erilaisia menetelmiä, kuten solujen kasvua ohjaavia kasvualustoja ja kemiallisia ärsykkeitä. Niidenkään avulla ei kuitenkaan ole onnistuttu tuottamaan täysin kypsiä sydänlihassoluja. Tämän tutkimuksen tarkoitus oli selvittää, kuinka ihmisen uudelleenohjelmoiduista kantasoluista erilaistettujen sydänlihassolujen viljeleminen polyetyleenitereftalaatti (PET) tekstiileillä vaikuttaa niiden geenien ilmentymiseen, toiminnallisuuteen ja rakenteellisiin ominaisuuksiin.

Ihmisen uudelleenohjelmoituja kantasoluja erilaistettiin sydänlihassoluiksi pien-molekyyli-menetelmällä ja saaduista soluista eroteltiin sydänlihassolut, jotka siirrettiin kasvamaan gelatiinilla päällystetyille PET tekstiileille 11-12 päiväksi. Kontrollisoluja viljeltiin gelatiinilla päällystettyjen peitinlasien päällä. TNNT2 geenin ilmentymistä tutkittiin molekulaarisen kypsymisen merkkinä qPCR:n avulla ja solujen toiminnallisuutta ja kalsiumin kierrätystä tutkittiin kalsiumkuvantamisen avulla. Solujen rakenteellisia ominaisuuksia tutkittiin immunosytokemiallisten värjäyksen ja fluoresenssi-kuvantamisen avulla, ja kuvista analysoitiin solujen muotoa, sarkomeerien orientaatiota ja pituutta CytoSpectre ohjelman avulla.

Solujen kasvattaminen PET tekstiileillä vaikutti parantavan niiden molekulaarista, toiminnallista ja rakenteellista kypsyyttä. Tekstiileillä viljellyt solut ilmensivät TNNT2 geeniä 3.35-kertaisesti verrattuna peitinlaseilla kasvatettuihin soluihin. Niillä esiintyi vähemmän epänormaalia kalsiumin kierrätystä, kalsiumin poisto solulimasta oli nopeampaa ja niillä oli keskimäärin nopeampi sykkimistahti, kuin kontrollisoluilla. Myös solujen muoto ja sarkomeerien orientaatio oli parempi. Toisaalta, kalsiumin vapautuminen solulimaan oli hitaampaa kuin kontrollisoluilla. Viljely PET tekstiileillä ei myöskään vaikuttanut sarkomeerien pituuteen, vaan sarkomeerit olivat selvästi lyhyempiä, kuin aikuisen sydänlihassoluissa.

PREFACE

This Master's thesis was done for Heart group as a part of Tekes project Human Spare Parts. Heart groups is a research group in BioMediTech, which is a joint institute of University of Tampere and Tampere University of Technology.

At first, I want to thank Katriina Aalto-Setälä, the leader of Heart group, for the opportunity to participate to the work done in her group. I want to thank my supervisor Mari Pekkanen-Mattila for guidance and support regarding the practical work as well as writing my thesis. I am also thankful for Risto-Pekka Pölönen for performing calcium imaging with me and helping me with processing the calcium imaging and immunostaining data. I would like to thank Minna Kellomäki for her valuable time.

Furthermore, I want to thank Henna Lappi for guidance in cell differentiation, culturing and cell sorting. Thank you Janne Koivisto for advice regarding my thesis and Elina Talvitie for preparing the textile samples. I would also like to thank the whole Heart group for welcoming me to work in the group.

Finally, I want to thank my family and friends for support throughout my studies.

Tampere, 7.3.2018

Martta Häkli

TABLE OF CONTENTS

LIST OF FIGURES

LIST OF TABLES

LIST OF SYMBOLS AND ABBREVIATIONS

3D	three dimensional
ATP2A2	sarco-endoplasmic reticulum Ca^{2+} ATPase transporting 2 encoding gene
AV node	atrioventricular node
BRY	T-brachyury
BSA	bovine serum albumin
CACNA1C	calcium voltage-gated channel subunit alpha 1 C encoding gene
CACNA1D	calcium voltage-gated channel subunit alpha 1 D encoding gene
CALR	calreticulin encoding gene
CASQ2	calsequestrin encoding gene
CAV3	caveolin 3 encoding gene
cDNA	complementary DNA
CICR	calcium-induced calcium release
CM	cardiomyocyte
CVD	cardiovascular disease
Cx43	connexin-43 encoding gene
EB	embryoid body
ECM	extracellular matrix
END-2	mouse visceral endoderm-like cell line
ESC	embryonic stem cell
FACS	fluorescent-activated cell sorting
GAPDH	glyceraldehyde-3-phosphate dehydrogenase encoding gene
GATA4	GATA binding protein 4 encoding gene
HAND1	heart and neural crest derivatives expressed 1 encoding gene
HAND2	heart and neural crest derivatives expressed 2 encoding gene
HCN4	hyperpolarization-activated cyclic nucleotide gated potassium channel 4 encoding gene
hiPSC	human induced pluripotent stem cell
hiPSC-CM	human induced pluripotent stem cell-derived cardiomyocyte
hPSC	human pluripotent stem cell
IFC	integrated fluidic circuit
IP3R	inositol triphosphate receptor encoding gene
iPSC	induced pluripotent stem cell
iPSC-CM	induced pluripotent stem cell derived-cardiomyocyte
ISL1	ISL LIM homeobox 1
JPH2	junctophilin encoding gene
KCND3	voltage-gated potassium channel subfamily D member 3 encoding gene
KCNH2	voltage-gated potassium channel subfamily H member 2 encoding gene
KCNQ1	voltage-gated potassium channel subfamily Q member 1 encoding gene
KDR	kinase insert domain receptor encoding gene
MACS	magnetic-activated cell sorting
MEF2C	myocyte enhancer factor 2C encoding gene
MIXL1	mix paired-like homeobox encoding gene
MyBPC	myosin binding protein C
MYH6	myosin heavy chain 6 encoding gene

MYH7	myosin heavy chain 7 encoding gene
MYH9	myosin heavy chain 9 encoding gene
MYL2	myosin light chain 2 encoding gene
MYL7	myosin light chain 7 encoding gene
NCX	sodium calcium exchanger encoding gene
NDS	normal donkey serum
NKX2.5	NK2 homeobox 5 encoding gene
PCL	poly-ε-caprolactone
PCR	polymerase chain reaction
PEG	polyethylene glycol
PET	polyethylene terephthalate
PLN	phospholamban encoding gene
PRKAG1	protein kinase AMP-activated non-catalytic subunit gamma 1 encoding gene
PRKAG2	protein kinase AMP-activated non-catalytic subunit gamma 2 encoding gene
PSC	pluripotent stem cell
qPCR	quantitative polymerase chain reaction
RGD	arginyl-glycyl-aspartic acid cell adhesion motif
RPMI/B27-I	insulin-free RPMI/B27
RT-STA	reverse transcription-specific target amplification
RYR	ryanodine receptor
RYR2	ryanoid receptor type 2 encoding gene
SA node	sinoatrial node
SCN5A	sodium voltage-gated channel alpha subunit 5 encoding gene
SERCA	sarco-endoplasmic reticulum Ca^{2+} ATPase
SOD1	superoxide dismutase 1 encoding gene
SR	sarcoplasmic reticulum encoding gene
TBX5	T-box 5
TCP	tissue culture polystyrene
TNNC1	slow skeletal and cardiac type troponin C1 encoding gene
TNNI1	slow skeletal type troponin I1 encoding gene
TNNI2	fast skeletal type troponin I2 encoding gene
TNNI3	cardiac type troponin I3 encoding gene
TNNT2	cardiac troponin T type 2 encoding gene
TRDN	triadin
T-tubule	transverse tubule

1. INTRODUCTION

Cardiovascular diseases (CVDs) include several disorders related to heart and blood vessels and are globally the number one cause of morbidity and mortality. Disorders causing damage either directly or indirectly to heart tissue comprise coronary heart disease, rheumatic heart disease and congenital heart disease, for example (World Health Organization 2017). CVDs include also cardiomyopathies, diseases where the contractile strength of the heart is compromised. In these diseases, the underlying mechanism may not be the same with all patients, who are still diagnosed with a single disease due to similar symptoms. Thus, effective medications and dosages vary among the patients (Tzatzalos et al. 2016), which creates a need for patient-specific disease models for genetic and other cardiac disease modeling on an individual basis (Hirt, Hansen & Eschenhagen 2014).

Human induced pluripotent stem cells (hiPSCs) can be produced from the patient's own somatic cells and differentiated into cardiomyocytes (CMs). hiPSC-derived CMs (hiPSC-CMs) reflect the genotype of the patient making it possible to develop patient- and disease-specific models to better understand the disease mechanism and evaluate therapeutic options (Hirt, Hansen & Eschenhagen 2014; Smith et al. 2017; Tzatzalos et al. 2016). hiPSC-CMs have several advantages over primary CMs, including minimal invasiveness in harvesting them and the possibility of unlimited supply of human CMs (Karakikes et al. 2015). Primary CMs are difficult to obtain due to invasive biopsies, difficult to dissociate into single cells and they have poor long-term survival in culture conditions (Sharma et al. 2015; Yang, Pabon & Murry 2014). However, *in vitro* cultured iPSC-CMs have an important disadvantage, as they are developmentally immature compared to CMs found in adult heart. This makes it difficult to relate the collected data to the actual disease, since phenotypically immature iPSC-CMs probably cannot accurately recapitulate the disease development (Smith et al. 2017).

There have been different approaches to obtain more mature hiPSC-CMs, including culturing the CMs on topographical culture substrates (Rao et al. 2013), extracellular matrix (ECM)-mediated maturation (Herron et al. 2016) as well as co-culturing with other cell types (Masumoto et al. 2016). Heart group at BioMediTech has studied structural maturation of hiPSC-CMs by culturing the cells on polyethylene terephthalate (PET) textiles coated with gelatin. Resulting hiPSC-CMs were more adult-like in shape and had more oriented sarcomere structure than the reference cells cultured on gelatin-coated coverslips. Also, the amount of multinucleated cells was higher (Junnila 2016). In the experiment, the attachment of the cells on the PET textiles was quite poor, leading to another study conducted by Mansikkala to discover if another coating material would improve

the cell attachment and maturation on the PET textiles. PET textiles were coated with gelatin, collagen, Matrigel and Geltrex. There were no great differences between the coating materials, but it was determined that Geltrex and Matrigel were slightly better for hiPSC-CM attachment and maturation (Mansikkala 2017).

This thesis continues the work done in Junnila's and Mansikkala's theses (Junnila 2016, Mansikkala 2017) by studying whether gene expression and functionality of hiPSC-CMs can be affected by culturing them on gelatin-coated PET. Gene expression was evaluated via qPCR and the functionality of the cells via calcium imaging. Also, structural maturation markers, such as cell shape and sarcomere orientation, were evaluated via immunostaining and fluorescence imaging. We expected that the gene expression, functionality and structural properties of the hiPSC-CMs grown on PET textiles resembles more that of adult human CMs.

2. LITERATURE REVIEW

2.1 Structure and function of heart and cardiomyocytes

Heart is a part of the cardiovascular system and pumps blood through the circulatory system. Circulatory system is divided into two distinct parts called pulmonary and systemic circulation. Pulmonary system circulates blood from heart to lungs for oxygenation and from lungs back to heart. Systemic circulation conveys oxygenated blood from the heart to other tissues of the body and from the other tissues back to heart (Hossler 2014, pp. 303; Moreau et al. 2002, pp. 84; Ross & Pawlina 2016, pp. 405). Heart is composed of heart wall, fibrous skeleton, conducting system and coronary vasculature. In addition, it is surrounded by pericardium, a tough fibrous sack consisting of two layers, of which the inner layer is in contact with heart wall. Pericardial space, the cavity between the layers of pericardium, is filled with serous fluid (Ross & Pawlina 2016, pp. 406). Figure 2.1 shows the structure of heart.

Heart consists of four chambers, including two atria and two ventricles. Blood enters the right atrium from systemic circulation via superior and inferior *venae cavae* and flows to the right ventricle where it is pumped to pulmonary circulation through pulmonary arteries. Pulmonary veins lead the blood from pulmonary circulation to the left atrium, from where it flows to the left ventricle to be pumped back to aorta and systemic circulation. The four valves in heart prevent blood flowing into the wrong direction. Mitral valve is located between the right atrium and ventricle and aortic valve between the right atrium and aorta. Tricuspid valve is between the left atrium and ventricle and pulmonary valve between the right ventricle and main pulmonary artery (Moreau et al. 2002, pp. 86; Ross & Pawlina 2016, pp. 406). The valves are attached to fibrous rings surrounding the valve orifices (Ross & Pawlina 2016, pp. 406).

Heart wall is composed of three distinct layers. Epicardium is the outermost layer connected to the inner pericardial layer of the fibrous sack. It consists of epithelial layer and connective tissue. Myocardium, the thick middle layer, consists of cardiac muscle. The innermost layer, endocardium, consists of endothelium and connective tissue. The conduction system of heart is located in this layer (Hossler 2014, pp. 354-355; Moreau et al. 2002, pp. 84; Ross & Pawlina 2016, pp. 407-408).

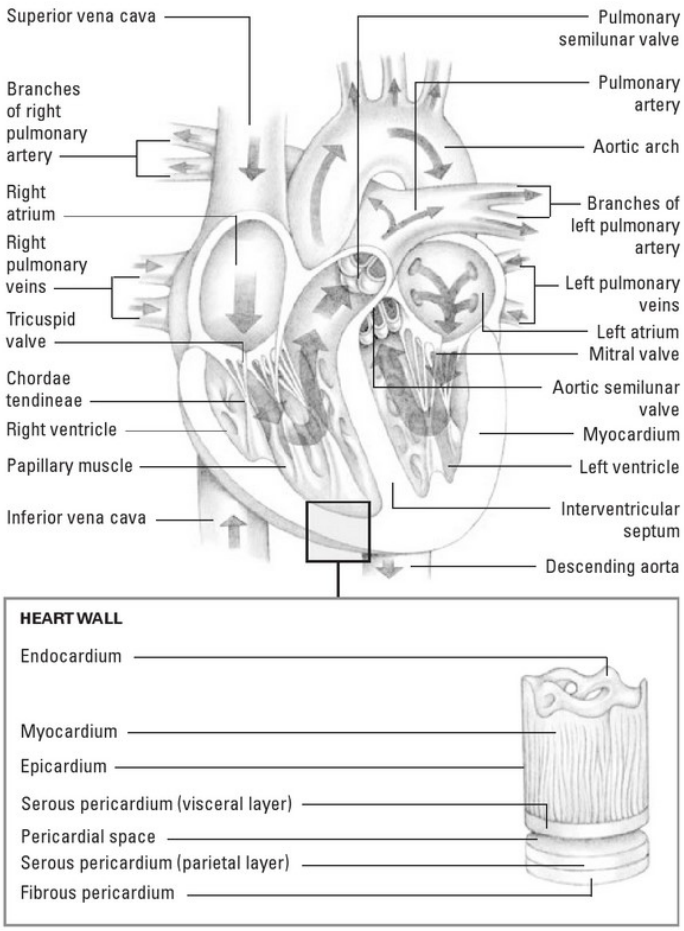

Figure 2. 1 *Structure of heart (Moreau et al. 2002, pp. 85). Heart consists of four chambers and four valves, and is composed of heart wall, fibrous skeleton, conducting system and coronary vasculature.*

The conduction system is formed by specialized conducting CMs and consists of two nodes and conduction fibers or bundles. It ensures the contraction of the heart muscle in a coordinated, rhythmic manner. Electrical impulses are generated at sinoatrial (SA) node, the pacemaker of heart. After impulse initiation at the SA node, it is conducted to the atrioventricular (AV) node and carried across the fibrous skeleton by AV bundle of His. From there, the conduction system divides into the right and left bundles and further into Purkinje fibers (Moreau et al. 2002, pp. 86-87; Ross & Pawlina 2016, pp. 409-410). Figure 2.2 shows the conduction system of the heart.

Cardiomyocytes, the cells responsible for contraction of the heart, are in the myocardium. Adult CMs are cylindrical in shape and have diameter of approximately 10-35 µm and length of approximately 100-150 µm. CMs form branched muscle fibers by connecting to adjacent cells via intercalated disks, which is a feature unique to CMs. CMs are striated due to the myofibril structure and have one or two slightly elongated nuclei in the center of the cell (Sarantitis et al. 2012; Severs 2000). The structure of the cells is highly organized due to longitudinal myofibril alignment, leading also to the alignment of other organelles according to them. Only about 0.1 % of the CMs in heart are capable of dividing,

which is why they are not considered renewing cells. Still, some regeneration after injury is possible (Ross & Pawlina 2016, pp. 333; Woodcock & Matkovich 2005).

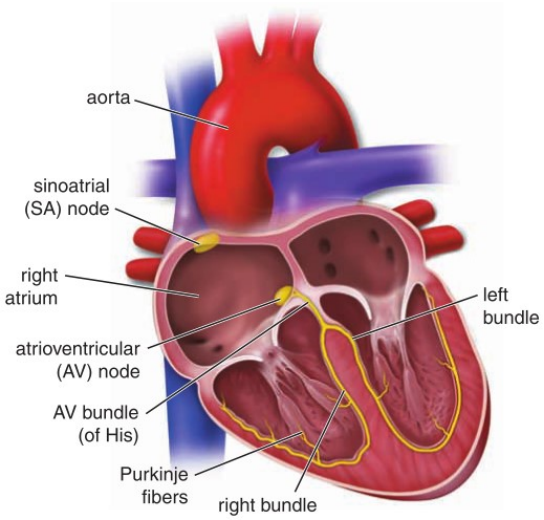

Figure 2. 2 *Conduction system of heart consists of sinoatrial node, atrioventricular node, AV bundle of His, right and left bundles and Purkinje fibers (Ross & Pawlina 2016, pp. 405).*

Myofibrils are the contractile structures in CMs. The smallest contractile unit of a myofibril is called sarcomere and its main components are thick myosin and thin actin filaments and titin. Thick filaments attach to the M-line and are composed of myosin and accessory protein called myosin binding protein C (MyPBC). Myosin consists of heavy chain and regulatory and essential light chains. M-line is composed of proteins myomesin and M-protein obscurin. Thin filaments are composed of actin, tropomyosin and troponin (I, C and T subunits) and attach to Z-line consisting of alpha actinin. Titin acts as a spring during contraction and relaxation and helps the thick filaments to stay in right arrangement between the thin filaments. Titin is attached to the Z-line and MyBPC of the thick filaments. (Golob, Moss & Chelser 2014; Ross & Pawlina 2016, pp. 321-322; Sarantitis et al. 2012) Figure 2.3 illustrates the myofibril and sarcomere structure.

Sarcomere resting length of adult CMs is approximately 2.2 µm (Sarantitis et al. 2012). Sarcomeres can be divided into I-, H- and A-bands and the striations of the cells originate from the alternating bands. I-band is the area around the Z-line where only thin filaments are present, while H-band is the area around the M-line where only thick filaments are present. A-band is the area where thick filaments are present, including the area where the thin and thick filaments overlap. The contraction of the cell is based on shortening of the sarcomeres due to increased overlap of thick and thin filaments leading to shortening of I- and H-bands. Simultaneous contraction of sarcomeres of a myofibril cause contraction of the myofibril and further the contraction of the cell (Ross & Pawlina 2016, pp. 319-325).

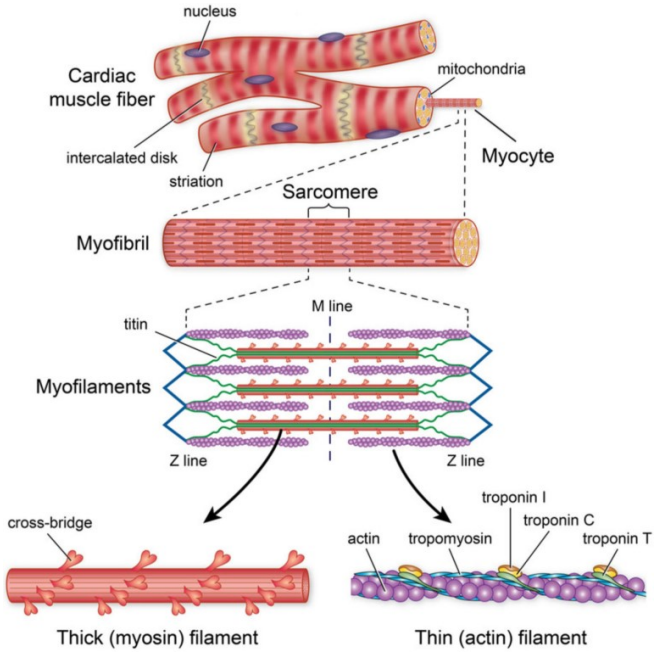

Figure 2. 3 *Sarcomere structure of cardiomyocytes, adapted from (Golob, Moss & Chelser 2014). Sarcomeres are composed of thick and thin filaments, cell contraction occurs, when the filaments slide interlocked.*

Contraction of CMs starts as calcium ions are released into the cytoplasm. Depolarization of sarcolemma, the cell membrane of CMs apart from intercalated disks, causes the release of calcium ions into cytoplasm through voltage-gated L-type calcium channels from invaginations of sarcolemma called transverse tubules (T-tubules). The increase in cytoplasmic calcium concentration induces calcium ion release into the cytoplasm from sarcoplasmic reticulum (SR), a network of interconnected membranous tubules surrounding each myofibril. The calcium release from SR is mediated by ryanodine receptors (RYRs), of which, type 2 RYR is the most abundant in CMs. This series of events is called calcium-induced calcium release (CICR) (Ross & Pawlina 2016 pp. 334-335; Severs 2000; Woodcock & Matkovich 2005). Figure 2.4 illustrates the structure of cardiac muscle fiber structure in more detail.

As calcium concentration increases in the cytoplasm, calcium ions bind to troponin, which in turn acts on tropomyosin to reveal binding sites for myosin heads on actin filaments. The myosin filaments then attach to actin and crawl along the thin filaments towards the Z-line shortening the sarcomere length and causing cell contraction (Ross & Pawlina 2016, pp. 319-325). After contraction, calcium ions are removed from the cytoplasm via sarco-endoplasmic reticulum calcium transporter (SERCA) and extrusion through the sarcolemma via Na^{+}-Ca^{2+}-exchanger (Woodcock & Matkovich 2005).

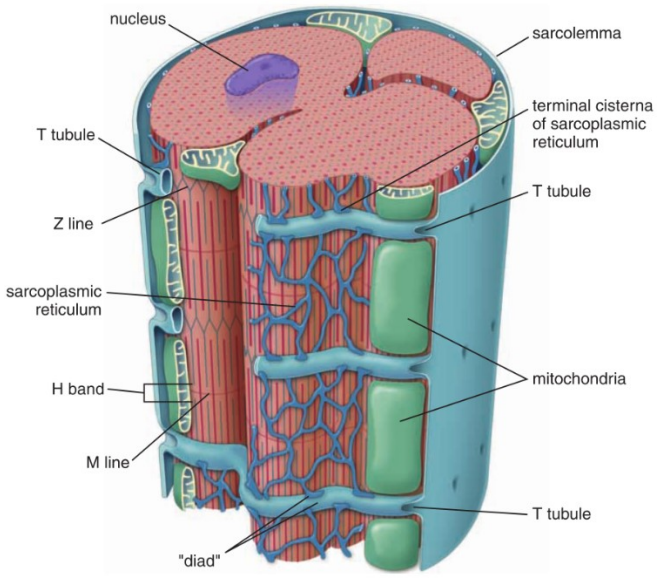

Figure 2. 4 *Structure of a cardiac muscle fiber. T-tubules are located in the level of Z-lines and sarcoplasmic reticulum surrounds the myofibrils. Organelles are aligned according to the mofibrils leading to a highly organized structure (Ross & Pawlina 2016, pp. 332).*

CMs are connected to each other via intercalated disks, highly specialized attachment sites oriented transversely to the muscle fiber (Ross & Pawlina 2016, pp. 332; Sarantitis et al. 2012; Severs 2000) as shown in figure 2.3. The disks consist of short segments where transverse and lateral parts are arranged in a step-like fashion (Ross & Pawlina 2016, pp. 332; Sarantitis et al. 2012). Functional components include three types of cell junctions. Fascia adherens and desmosomes are anchoring junctions while gap junctions enable direct communication between the cells. Fascia adherens are major components of the transverse parts of intercalated disks and responsible for attachment of myofibrils to the cell membrane at the both ends of the CMs. Desmosomes, on the other hand, are found in both transverse and lateral parts of the intercalated disks and are responsible for binding individual muscle cells together (Ross & Pawlina 2016; Sarantitis et al. 2012; Severs 2000).

Gap junctions are formed by two connexons, which in turn are formed by six connexin proteins. Each connexon penetrates one cell membrane and are joined together in extracellular space to form the gap junction (Ross & Pawlina 2016, pp. 131; Severs 2000). Connexin-43 is the most abundant connexin type in atrial and ventricular myocardium, although many connexin types have been discovered and connexin-45 and -40 are also present in CMs in different quantities (Sarantitis et al. 2012; Severs 2000). Figure 2.5 shows the general structure of a gap junction.

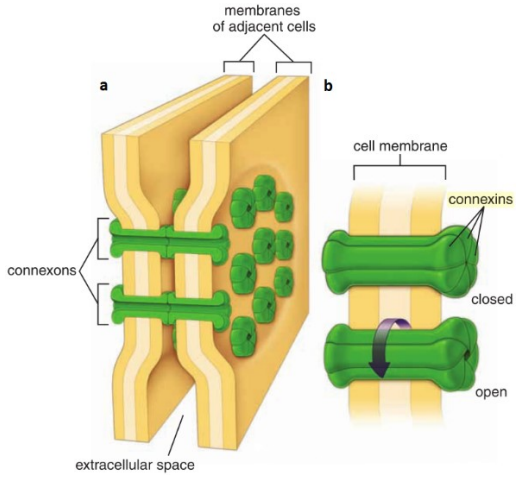

Figure 2. 5 *Structure of a gap junction, adapted from (Ross & Pawlina 2016, pp. 131). a) Two connexons form a gap junction through the cell membranes of two adjacent cells. b) One connexon is formed of six connexin proteins.*

Gap junctions are major components of the lateral parts of intercalated disks. The junctions enable communication between adjacent cells including rapid conduction of action potentials as well as direct transmission of chemical signals, allowing the muscle fibers to behave synchronically (Ross & Pawlina 2016, pp. 334; Sarantitis et al. 2012; Severs 2000). Also, the non-cardiomyocyte cells of myocardium can participate in this type of cell communication. In addition to CMs, for example fibroblasts are found in myocardium. These two cell types produce the ECM of the myocardium, which has a crucial role in dynamic interactions between the CMs. The ECM in myocardium is located in the endomysium, connective tissue surrounding the individual cardiac muscle fibers. (Sarantitis et al. 2012)

2.2 Overview of stem cells

Stem cells are unspecialized cells characterized by their ability to self-renewal and differentiation into specialized cells (Daley 2015; Dulak et al. 2015; Kalra & Tomar 2014). They are studied for the wide range of applications they could be used in, including tissue regeneration of damaged or failing tissues and treating immunodeficient diseases and cancer (Yin, Han & Lee 2016). Furthermore, they can be utilized in drug development and testing as well as in disease modeling after differentiation into the wanted cell type (Smith et al. 2017). Stem cells can be classified based on their potency, which is their ability to differentiate into cells of multiple lineages, or on the basis of their source (Daley 2015; Kalra & Tomar 2014).

Totipotent stem cells are stem cells able to differentiate into all possible cell types, including extraembryonic tissues, such as fetal membranes and placenta. The first few cells resulting from the division of fertilized zygote are considered as totipotent (Daley 2015;

Kalra & Tomar 2014). Pluripotent stem cells can differentiate into cells of all three embryonic lineages called ectoderm, mesoderm and endoderm, meaning that they can form any other tissue types, except for extraembryonic tissues. Pluripotent stem cells (PSCs) include embryonic stem cells (ESCs) isolated from the inner cell mass of blastocysts 4-5 days after fertilization and induced pluripotent stem cells (iPSCs), which are somatic cells reverted back to embryonic stem cell-like state (Daley 2015; Dulak et al. 2015; Kalra & Tomar 2014).

Multipotent stem cells can differentiate into many cell types within a particular lineage and form specialized cells of a specific tissue. These include hematopoietic stem cells that are able to differentiate into blood cells (Daley 2015; Dulak et al. 2015; Kalra & Tomar 2014). Oligopotent stem cells are not always defined as their own stem cell type, but this group includes stem cells with the ability to differentiate into a few cell types. For example, lymphoid and myeloid stem cells are considered oligopotent. Unipotent stem cells can produce cells of their own type. For example muscle stem cells are unipotent (Kalra & Tomar 2014). Unipotent stem cells differ from progenitor cells in their ability to self-renewal. Progenitor cells typically are able to differentiate into one cell type but lack the capability to self-renewal, which separates them from stem cells (Dulak et al. 2015).

Stem cells can also be classified based on their source, in which case there are three distinct groups. Embryonic stem cells are pluripotent self-replicating and potentially immortal stem cells. Adult stem cells are multi- or unipotent stem cells that can be found after embryonic development throughout the body. Their primary function is to maintain and repair tissues (Kalra & Tomar 2014). Induced pluripotent stem cells can be produced from somatic cells by reprogramming them to an embryonic-like state with four factors, Oct3/4, Sox2, c-Myc and Klf4 under embryonic stem cell culture conditions. iPSCs have properties similar to embryonic stem cells and have been produced at first from mouse (Takahashi & Yamanaka 2006) and later from human adult fibroblasts (Takahashi et al. 2007) and other somatic cells (Smith et al. 2017).

2.3 Differentiation of hiPSCs into cardiomyocytes

hiPSCs can be differentiated into CMs with several methods, including embryoid body (EB) formation-based differentiation, co-culture-based differentiation on feeder cells and monolayer culture-based differentiation (Mummery et al. 2012; Talkhabi, Aghdami & Baharvand 2016). Figure 2.6 summarizes the different methods used. Differentiation based on EB formation is spontaneous and was the first method to produce beating cardiomyocytes (Smith et al. 2017). It has been the most commonly used method for performing functional studies as well as studying disease mechanisms in CMs (Di Pasquale, Song & Condorelli 2013; Smith et al. 2017).

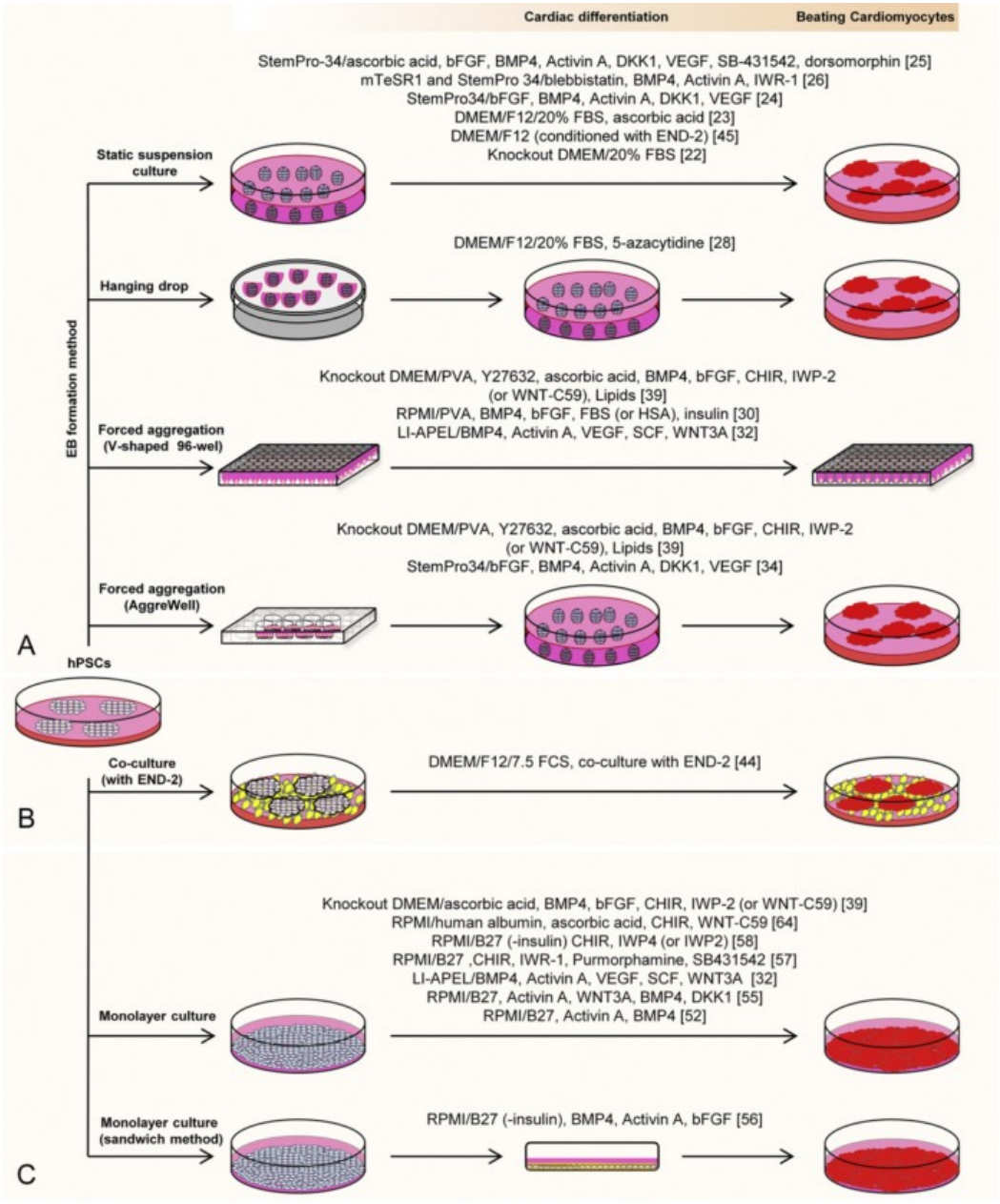

Figure 2. 6 *Different methods available to differentiate human pluripotent stem cells into cardiomyocytes include EB formation, co-culture with feeder cells and monolayer culture-based differentiation (Talkhabi, Aghdami & Baharvand 2016).*

EB formation-based differentiation. EBs are multicellular spheroids formed by PSCs under certain culture conditions, such as static suspension culture, hanging drop and forced aggregation conditions. These aggregates do not support pluripotency, but the PSCs start to form an inner layer of ectoderm-like cells and a single outer layer of endoderm, differentiating into cells of all three germ layers, including CMs (Mummery et al. 2012; Talkhabi, Aghdami & Baharvand 2016). This method is straightforward, economical, easily practicable and suitable for all cell lines (Di Pasquale, Song & Condorelli 2013) but low efficiency and variability between the cell lines are seen as disadvantages (Mummery et al. 2012; Talkhabi, Aghdami & Baharvand 2016).

To achieve more efficient CM differentiation, EB formation-based differentiation has been developed and optimized with different media and growth factors. Burridge *et al.* used forced aggregation EB formation with chemically defined medium containing optimized concentrations of mesodermal morphogens BMP4 and FGF2, polyvinyl alcohol, serum and insulin. In addition, the culture was exposed to 5 % oxygen concentration. In nine days after the initial aggregation, the acquired EBs consisted of 64-89 % of beating CMs. In contrast, the commonly used basic protocol yields only 1-25 % of CMs in 30 days (Burridge et al. 2011).

Co-culture-based differentiation. Co-culture-based differentiation of hiPSCs into CMs relies on a characteristic of early cardiac development, when the visceral endoderm posterior to embryonic cardiac crescent initiates cardiogenesis by providing inductive and inhibitory signals required for cardiac development. Thus, co-culturing PSCs with mouse visceral endoderm-like cell line (END-2) can be utilized in derivation of CMs from PSCs (Mummery et al. 2012; Talkhabi, Aghdami & Baharvand 2016). Another cell line inducing PSC differentiation into CMs is OP9, a stromal cell line from mouse bone marrow (Mummery et al. 2012; Narazaki et al. 2008). The mechanism of the CM differentiation induced by the END-2 cells is still not fully understood, but it is known that the cell-cell interactions are not vital in the process, since END-2 conditioned medium alone has been proven to induce PSC differentiation into CMs (Talkhabi, Aghdami & Baharvand 2016).

Initially, co-culturing of PSCs with END-2 cells produced beating areas into only 35 % of the wells, and of those areas only 2-3 % were CMs (Mummery et al. 2012). Thus, the method was modified to achieve better yield of CMs by changing to serum- and insulin-free defined medium. This way, the amount of beating colonies increased ten-fold and each colony consisted of approximately 25 % of CMs (Mummery et al. 2012; Talkhabi, Aghdami & Baharvand 2016). Even though the method is reliable for producing CMs from many hPSC lines, it is time consuming and laborious (Talkhabi, Aghdami & Baharvand 2016) and has difficulties in yielding pure CM populations (Kreutzer et al. 2014).

Monolayer culture-based differentiation. Monolayer culture-based CM differentiation utilizes the epithelial cell-like morphology hiPSCs have in adherent culture systems (Talkhabi, Aghdami & Baharvand 2016). This method has an advantage over EB formation-based differentiation, since the relatively uniform monolayer of cells does not have the diffusional barriers present in EBs. Thus, application of growth factors and other interventions should be more controllable and reproducible (Mummery et al. 2012; Smith et al. 2017; Talkhabi, Aghdami & Baharvand 2016). Efficient induction of CM differentiation depends on the seeding density of the hiPSCs (Burridge, Holmström & Wu 2015) as well as on the right combination and dose of growth factors applied at the right time (Talkhabi, Aghdami & Baharvand 2016).

Monolayer culture-based CM differentiation is induced by changing mouse embryonic fibroblast (MEF) conditioned medium, where the hiPSCs are cultured in as a confluent monolayer, into insulin-free RPMI/B27 medium. The cells are treated with a high dose of Activin A for one day and subsequently with BMP4 for four days (Mummery et al. 2012; Smith et al. 2017; Talkhabi, Aghdami & Baharvand 2016). With Percoll gradient centrifugation step, the purity of CMs in the culture was increased to 82 % (Mummery et al. 2012; Talkhabi, Aghdami & Baharvand 2016). Ye *et al.* used also vascular endothelial growth factor in differentiation after Activin A and BMP4 treatment, which further increased the yield to over 85 % of CMs (Ye et al. 2013). Furthermore, Matrigel can be used to coat the cells after they have reached 90 % confluence (Mummery et al. 2012; Talkhabi, Aghdami & Baharvand 2016). Matrigel is a commercialized matrix material consisting mostly of laminin-111, collagen IV, entactin and heparan sulfate, and used for example as a substrate for cell culturing and in various assays (Benton et al. 2014). Coating cells is called the sandwich method and has been shown to result in efficient generation of CMs from multiple hiPSC lines with high yield and CM purity of 98 % (Mummery et al. 2012; Talkhabi, Aghdami & Baharvand 2016).

Small molecule mediated differentiation. hiPSC monolayer culture can be utilized also in small molecule mediated differentiation. The differentiation into CMs is based on modulating Wnt/β-Catenin signaling. First, Wnt signaling is made more active with GSK3B inhibitor, for example CHIR99021, and then suppressed two days later with Wnt inhibitor, for example IWP-4 (Burridge, Holmström & Wu 2015; Sharma et al. 2015). In this method, hiPSCs are cultured for example in mTeSR1 medium until they are a confluent monolayer, after which the differentiation is started (Karakikes et al. 2014; Sharma et al. 2015). GSK3B and Wnt inhibitors are introduced to the cells in insulin-free RPMI/B27 medium, which is later changed to RPMI/B27 medium with insulin (Sharma et al. 2015).

The hiPSC-CMs generated this way express standard CM markers including cardiac troponin T and alpha actinin (Burridge, Holmström & Wu 2015; Sharma et al. 2015). Beating CMs are achieved in seven to ten days with 50 % yield. Advantages of small molecule mediated monolayer differentiation include higher efficiency and cost-effectiveness due to decreased need for expensive growth factors (Sharma et al. 2015). In addition, using small molecules can provide more reproducible results (Denning et al. 2016; Mummery et al. 2012). On the other hand, timing of the small molecule application is critical in this method (Mummery et al. 2012).

2.4 Enriching hiPSC-derived cardiomyocyte culture

Cell separation methods are used to separate cells of a specific type from heterogeneous samples containing multiple different cell types, lineages and cell maturation and activation states at varying proportions. Separating the cell type of interest is important, for example, in transcriptomic and proteomic studies, since performing these analyses on

heterogeneous biological samples can lead to misrepresented or incorrect results if the information of interest concerns a small cell population only. Whole sample analysis could diminish or even mask the specific features of the target cells, thus preventing sufficient characterization and identification of molecular mechanisms taking place in them. (Almeida, García-Montero & Orfao 2014)

Cells can be separated from each other based on different properties, which have traditionally been cell adherence properties, density and size, morphological characteristics and antibody-binding, immunophenotypic properties. Some newer methods based on microfluidic technologies taking advantage of other characteristics of the cells have also been introduced. These characteristics include cell elasticity in response to acoustic waves and membrane polarization in nonuniform electrical field (Almeida, García-Montero & Orfao 2014; Shields IV, Reyes & López 2015). Different methods have different advantages and disadvantages related to purity, recovery, yield, efficiency, cell viability, sample volume and throughput speed (Almeida, García-Montero & Orfao 2014).

In case of CMs, purification of cells based on differences in metabolic activity of CMs compared to other cell types can be utilized in enriching of the CMs in the culture. Sharma *et al.* used glucose starvation, which selectively eliminates other cells than CMs. This is due to the ability of CMs to utilize lactate as primary energy source, an ability the other cell types lack. The treatment resulted in 40 % increase in the ratio of CMs to other cell types (Sharma et al. 2015). Earlier, Tohyama *et al.* reported CM purification of up to 99 % from cell source consisting of only 10 % CMs using the similar glucose-starvation method. This method is easily applicable and requires only culturing CMs in low glucose medium (Tohyama et al. 2013). Ma *et al.* used a different CM purification method, and performed genetic modification-based purification using myosin heavy chain 6 (MYH6) gene to express blasticidin S resistance gene. The hiPSCs were engineered to exhibit blasticidin S deaminase downstream of the last exon of the native MYH6 gene (Ma et al. 2011).

Antibody-based cell sorting methods include flow cytometry-based fluorescence-activated cell sorting (FACS) and magnetic-activated cell sorting (MACS) (Almeida, García-Montero & Orfao 2014; Shields IV, Reyes & López 2015). FACS was invented by Herzenberg *et al.* in 1969 (Hulett et al. 1969) and later on optimized and developed into a technique that now has become a reference point for other cell sorting methods (Shields IV, Reyes & López 2015). MACS technology was commercialized in 1989 by Miltenyi *et al.* (Miltenyi et al. 1990) and has also become a widely used cell sorting technique (Almeida, García-Montero & Orfao 2014). These methods are very effective for isolation of viable cells with high purity, but have limitations regarding longer sorting times due to inability to work with large volume samples as well as lower cell recovery and yield (Almeida, García-Montero & Orfao 2014). Antibodies used for CM separation include VCAM1 and SIRPα (Iseoka et al. 2017; Schwach & Passier 2016).

FACS is based on the unique light scattering and fluorescence-associated features of the cells labeled with genetic manipulation or cell surface specific antibodies (Almeida, García-Montero & Orfao 2014; Schwach & Passier 2016; Shields IV, Reyes & López 2015). The cells are in suspension and pass through one or more light sources one by one. The cells are analyzed based on the mentioned features and subsequently separated from the sample. Purified cells can be directly placed into individual wells for example for cloning or polymerase chain reaction (PCR). Advantages of FACS include high purity and efficiency and rapidity of the process (Almeida, García-Montero & Orfao 2014). Still, genetic manipulation related to the labeling is time consuming and not feasible for every cell line. FACS has been widely utilized in purification of CMs from heterogeneous populations, but has several disadvantages including undesired contaminations as well as low viability of the target cells (Schwach & Passier 2016).

MACS technology is another option for antibody-based cell sorting. Here, magnetic beads are attached to antibody reagents so that the beads can bind to the cell surface epitopes of the cells of interest through antibody-mediated binding. The cells are then separated from suspension by passing the sample through a magnet, leading to removal of unwanted cells. The cells of interest can be collected to a separate place by turning off the magnet (Almeida, García-Montero & Orfao 2014; Miltenyi et al. 1990). Several types of beads are commercial for cell sorting, of which the most widely used are Dynabeads® and MACS® beads (Almeida, García-Montero & Orfao 2014). Due to the disadvantages related to FACS, MACS technology has been used for CM separation in several studies (Iseoka et al. 2017; Leung et al. 2015; Schwach & Passier 2016).

Dynabeads are magnetisable superparamagnetic (magnetic only in a magnetic field) polystyrene microbeads conjugated to specific antibodies. Their advantages include that they do not require separate or special sample preparation apart from sample incubation with the beads. The beads also allow negative selection of targeted cells, meaning that cells without certain surface marker can be selected when the absence of these markers is critical. When positive selection of the target cells is used, the detachment and removal of the beads is required to perform further analysis (Almeida, García-Montero & Orfao 2014; Neurauter et al. 2007). This can prove to be difficult, since polyvalent binding of the beads can lead to their endocytosis by labeled macrophages. Another disadvantage is slow binding capacity of antibody-conjugated beads due to larger particle size (Almeida, García-Montero & Orfao 2014).

MACS® beads are antibody-conjugated biodegradable iron-based nanoparticles. Since the beads are so small, this technology requires high-gradient magnetic cell separation columns that are filled with a matrix of ferromagnetic steel wool or iron spheres to capture the labeled cells in a strong magnetic field. The method can be utilized in both high throughput purification of large number of cells as well as in isolation of rare cells present in sample at low frequencies. Positive selection is most efficient way to isolate target cells

with high purity but negative selection can also be used depending on the cells of interest and the availability of suitable antibodies or their combinations. (Almeida, García-Montero & Orfao 2014)

2.5 Maturation of hiPSC-derived cardiomyocytes

Compared to adult human CMs, hiPSC-CMs exhibit immature phenotype and functionality limiting their usability in different applications (Bedada, Wheelwright & Metzger 2016; Denning et al. 2016; Huethorst et al. 2016; Lundy et al. 2013). There are different markers that have been determined to indicate the maturation state of CMs, but there are problems related to the reliability of some of these maturation markers, since they are susceptible to change and can revert to the immature state during stress (Bedada, Wheelwright & Metzger 2016). The maturation of hiPSC-CMs has be assessed based on structural, contractile and electrical properties as well as calcium handling properties and gene expression of the cells (Bedada, Wheelwright & Metzger 2016; Denning et al. 2016; Lundy et al. 2013). There are also different methods to improve the *in vitro* maturation of these cells (Denning et al. 2016).

2.5.1 Maturation markers of hiPSC-derived cardiomyocytes

Differences between hiPSC-CMs and adult CMs include structural properties, so they can be used to evaluate the maturity of hiPSC-CMs. hiPSC-CMs are small and round or multiangular cells typically with single nucleus, whereas adult CMs are rod-like, larger and 25-57 % of the cells are binucleated (Denning et al. 2016; Lundy et al. 2013). The aspect ratio of the hiPSC-CMs is (2-3):1 indicating that the cells do not have clear longitudinal axis. The aspect ratio of adult CMs, on the other hand, is (5-9):1 and the longitudinal axis can be clearly determined. Sarcomeres of hiPSC-CMs are disorganized and shorter than in adult CMs and sarcoplasmic reticulum is poorly developed and the sarcolemma exhibits no T-tubules (Denning et al. 2016). Figure 2.7 shows differences in hiPSC-CM and adult CM structure.

The poorly developed SR as well as the lack of T-tubules likely affect the calcium handling properties of hiPSC-CMs (Karakikes et al. 2015). In adult CMs, calcium influx via the L-type calcium channels initiates CICR and calcium is released from SR. The contractility is further increased by phosphorylation of the L-type channels, which in turn increases the calcium flux. After contraction, the calcium is taken back into SR (Bedada, Wheelwright & Metzger 2016). The release and uptake kinetics of calcium have been shown to be relatively slow in hiPSC-CMs compared to adult CMs and characterized by a U-shape calcium waveform suggesting immature calcium handling mechanisms (Karakikes et al. 2015; Lundy et al. 2013).

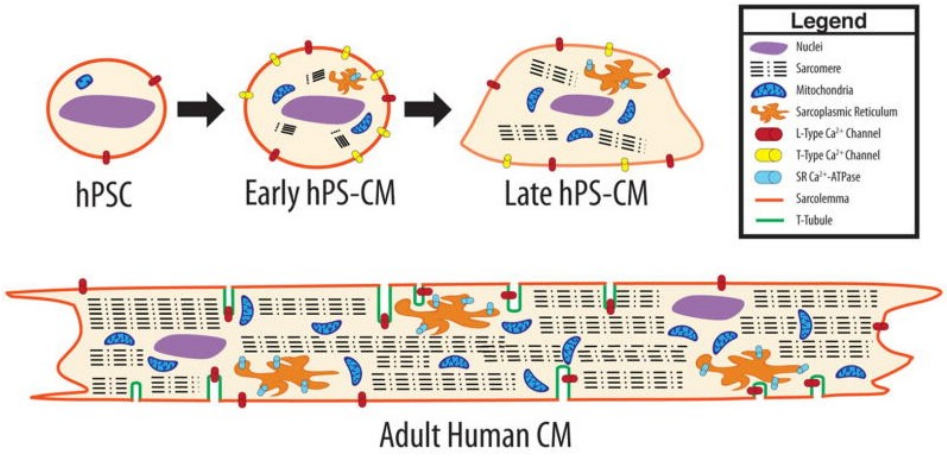

Figure 2. *7 Structural comparison of hPSC-CMs and adult CMs. Adult CMs are much larger, rod-like in shape and have highly organized structure, whereas hPSC-CMs are smalller, disorganized and exhibit no clear longitudinal axis (Robertson, Tran & George 2013).*

The immature structural properties of hiPSC-CMs partially cause the immaturity of their contractility pattern (Huethorst et al. 2016). The contraction force produced by hiPSC-CMs is clearly lower than that of adult CMs. Force produced by adult CM muscle stripes has been shown to be 40-80 mN/mm^2, which is at least ten times greater than force produced by three dimensional hiPSC-CM constructs (0,08-4 mN/mm^2). The contraction force produced by single adult CM is in range of micronewtons, whereas it is in range of couple hundred nanonewtons for single hiPSC-CMs (Denning et al. 2016). Force production and contractility are important parameters in CM function, since they determine how effectively the heart can circulate blood (Huethorst et al. 2016).

Immaturity of hiPSC-CMs can be evaluated from the electrical properties of the cells. hiPSC-CMs beat spontaneously while that is not observed in mature adult CMs due to high expression of hyperpolarization-activated pacemaker current I_f and low expression of inwardly rectifying potassium current. Also, some ion channels present in adult CMs have not been identified on hiPSC-CMs (Denning et al. 2016; Karakikes et al. 2015). The resting membrane potential is from -80 to -90 millivolts in adult CMs, whereas it is from -20 to -60 millivolts in hiPSC-CMs. Furthermore, the upstroke and conduction velocities are significantly lower in hiPSC-CMs (Denning et al. 2016).

There are also differences in metabolism between hiPSC-CMs and adult CMs. The metabolic phenotype of hiPSC-CMs resembles that of embryonic ventricular myocytes that use glycolysis of glucose and lactate for energy production. Adult CMs, on the other hand, use mainly fatty acids and produce energy from them by oxidative phosphorylation (Denning et al. 2016; Karakikes et al. 2015). Metabolic maturation has been tried to induce by culturing hiPSC-CMs with an adipogenic cocktail or glucose-free medium. hiPSC-CMs exhibiting more mature metabolic phenotype have been used in studying mitochondrial disorders (Karakikes et al. 2015).

2.5.2 Methods to improve hiPSC-derived cardiomyocyte maturity

Approaches to improve maturation of hiPSC-CMs cultured *in vitro* include topographical cues and substrate stiffness, medium additives, mechanical or electrical stimulation, genetic manipulation and co-culturing with other cell types (Denning et al. 2016). Lundy *et al.* also studied the effect of prolonged *in vitro* culturing on the structural and functional maturation of hiPSC-CMs to discover whether the cells can adopt more adult-like CM phenotype. In this experiment, late-stage hiPSC-CMs were cultured for 80-120 days and early-stage hiPSC-CMs were cultured for 20-40 days and the groups were compared with each other on the maturation point of view (Lundy et al. 2013).

In the experiment by Lundy *et al.* (2013) the late-stage hiPSC-CMs were more mature in morphology, as increased cell size and anisotropy were observed as well as greater myofibril density and alignment. Still, no T-tubule formation was detected. The number of multinucleated cells increased and contraction kinetics slowed, whereas the contracting magnitude of the cells had doubled during longer culture time. Also, calcium handling of the cells resembled more that of adult CMs' with increase in calcium release and uptake rates. Electrophysiological assessment in hiPSC-CMs revealed increase in action potential amplitudes and faster upstroke velocities (Lundy et al. 2013). Even though it is not practicable to use extended culture in routine biomedical applications (Denning et al. 2016), the experiment showed that hiPSC-CMs are capable of adopting more mature phenotype.

Topographical cues, such as culturing on grooved substrates or textiles can be used to improve maturation of hiPSC-CMs. Huethorst *et al.* (2016) investigated the effects of topographical gradient substrate on morphological and functional maturity of hiPSC-CMs. The depth of the grooves varied in one direction from deep to shallow and the distance between the grooves varied in the other direction from wide to narrow. The width of the grooves was constant. The cells were seeded homogenously on the substrate and cultured for ten days and the eccentricity, elongation, orientation, sarcomere length and contractility of the cells were measured at days four and ten. The deepest and narrowest region showed increased eccentricity, elongation and orientation compared to the control cells cultured on a flat substrate. In addition, the elongated cells in that area exhibited prolonged the contraction duration. It was also observed that cell density was higher in the middle region, suggesting that the cells had migrated towards a more favorable spot. It was hypothesized that the cells favor cell-cell contacts over topography, since in the deep narrow area the cell density was lower even though the cells there were more adult-like. (Huethorst et al. 2016)

Furthermore, a study conducted by Rao *et al.* showed that calcium handling properties of the hiPSC-CMs cultured on microgrooved substrates were altered due to improved sarcoplasmic reticulum calcium cycling associated with more organized SR (Rao et al. 2013). Also, Carson *et al.* found nanogrooved substrates coated with arginyl-glycyl-aspartic acid (RGD) sequence containing peptide to improve structural development of hiPSC-CMs (Carson et al. 2016).

Another topographical approach for hiPSC-CM maturation is culturing the cells on fiber or textile structures. Khan *et al.* studied changes in morphology and function of hiPSC-CMs cultured on an aligned nanofiber patch. Compared to reference culture on a flat surface, the cells cultured on the fibers were elongated and exhibited improved alignment. Also, the mitochondria and the myofibrils were aligned along the nanofibers. The calcium cycling rate was demonstrated to be faster in the CMs cultured on nanofibers resulting also in greater contraction frequency. On the other hand, no differences in electrical properties or gene expression were observed between the groups. (Khan et al. 2015)

Parrag *et al.* studied the effect of fiber alignment and co-culture with mouse embryonic fibroblasts on mouse embryonic stem cell-derived cardiomyocytes and suggested that it is not enough to culture the CMs on fibers but the fibers have to be aligned as well for the CMs to exhibit more oriented and adult-like phenotype (Parrag, Zandstra & Woodhouse 2012). Han *et al.* had similar results regarding the alignment of the fibers. However, they also deduced that cell alignment alone has a limited capability to enhance robust maturation of hiPSC-CMs (Han et al. 2016). In their study, they compared hPSC-CMs grown on aligned and random fibrous scaffolds and hPSC-CMs grown on flat tissue culture polystyrens (TCPs). They observed modest structural maturation and enhanced molecular maturation in cells grown on aligned fibrous scaffolds but no differences in levels of proteins associated to CMs or pharmacological responses to several cardioactive compounds were observed between cells of different culture scaffolds. Furthermore, the calcium transient kinetics were slower in hPSC-CMs cultured on the fibers than on TCP, suggesting incomplete maturation of the aligned cells and limited capability of the method in improving the CM maturation (Han et al. 2016).

Nunes *et al.* developed a platform called biowire that combines topographical and electrical cues to improve hiPSC-CM maturation. hPSC-CMs were cultured with endothelial cells, fibroblasts and smooth muscle cells on an electrically paced surgical suture for two weeks. The CMs aligned along the biowire axis increasing in size and adopting a rod-like shape. They were shown to strongly express cardiac contractile proteins alpha actinin, actin and cardiac troponin. Sarcomere structure was more organized with visible Z lines and H- and I-bands. Also the calcium handling properties of the cells were enhanced (Nunes et al. 2013) unlike in topographical maturation alone (Han et al. 2016). However, the lack of T-tubules and visible M-lines demonstrate that the CM maturation achieved with the biowire culturing is incomplete (Nunes et al. 2013).

Another study by Ruan *et al.* investigated how the combination of mechanical and electrical stimulation affects the maturation of hiPSC-CMs. Structural remodeling, contractility and calcium handling of the engineered heart tissue were assessed. It was observed that the cells responded to static stress with increased cell alignment, size, contractility and expression of calcium handling related proteins. When electrical pacing was included, the contractility increased further as well as the expression of calcium handling proteins. One important notice was increased twitch force due to increased length, a cellular basis of a fundamental characteristic of human heart called Frank-Starling mechanism. This was considered as an indication of the effectiveness of the method in producing realistic models of human myocardium. (Ruan et al. 2016)

Yet another approach for hiPSC-CM maturation has been ECM-mediated maturation, since ECM has a central role in cell-cell signaling and cell-ECM interactions, which are critical in CM development and maturation (Chun et al. 2015; Feaster et al. 2015; Herron et al. 2016). Feaster *et al.* demonstrated that culturing on Matrigel mattress produces hiPSC-CMs with relative morphological, molecular and functional maturation in five to seven days. This maturation method enables fast assessment of contractile and calcium handling properties of single cells relatively easily. The hiPSC-CMs acquired with this method can be useful for certain applications due to short culturing time despite the incomplete maturation regarding calcium handling properties of the cells (Feaster et al. 2015).

Herron *et al.* achieved similar results when they cultured hiPSC-CMs on Matrigel coated PDMS membranes. Conduction velocities of the hiPSC-CMs were measured to be two times faster than previously reported for hiPSC-CM monolayers, due to the optimal ECM combination. The electrophysiological and structural maturation included also formation of intercellular gap junctions, more mature myofilament isoform expression as well as increased expression of integrin beta 1 and alpha 5 receptor genes. Similarly to the results of Feaster *et al.* the maturation was achieved in only seven days (Herron et al. 2016).

Chun *et al.* studied combinatorial polymer matrices comprised of different ratios of poly-ε-caprolactone (PCL), polyethylene glycol (PEG) and carboxylated PCL in hiPSC-CM maturation. Especially the 4%PEG-96%PCL scaffold was reported to enhance the contractility and mitochondrial activity in hiPSC-CMs. Also, higher expression of cardiac myosin light chain-2v, cardiac troponin I and integrin alpha 7, which are considered as mature CM markers, were observed. It was suggested that the maturation was promoted by mimicking certain features in interactions between basement membrane-integrin and sarcolemma (Chun et al. 2015).

hiPSC-CM maturation can also be induced and modulated by medium additives, which is a simple, straightforward method, but they are unlikely to induce complete maturation of CMs and thus used in combination with other methods. Several factors have been

shown to induce hiPSC-CM maturity in different mechanisms. For example, triiodothyronine regulates isoform switching of several myocardial proteins and is essential for normal cardiac development. Also, a combination of insulin, dexamethasone and 3-isobutyl-1-methil-xanthine has been shown to enhance metabolic maturation by enhancing mitochondrial oxidative phosphorylation and increasing fatty acid synthesis. Other factors include insulin-like growth factor, corticosterone and eicosapentaenoic acid. Moreover, maturation can be enhanced by genetic manipulation, for example by forced expression of missing ion channels. (Denning et al. 2016)

2.6 Cardiac specific gene and protein expression

Gene expression can be evaluated to ensure successful differentiation into wanted cell type as well as in assessing the maturation state of the cells. Different cell types express different genes in different levels, which can be used to compare for example hiPSC-CMs to adult CMs. To do this, it is essential to know the genes characteristically expressed by the specific cell type. Next, genes expressed by adult human cardiomyocytes and the effects of different maturation methods on the expression of these genes by hiPSC-CMs are discussed.

2.6.1 Cardiomyocyte related genes and their expression in hiPSC-CMs

hiPSCs start to differentiate into CMs by a sequential expression of distinct set of genes with a pattern consistent with normal cardiac development (Karakikes et al. 2015). On the other hand, the gene expression of hiPSC-CMs has been shown to be similar to that of the CMs of first trimester fetal heart rather than that of adult CMs (Denning et al. 2016). According to Rao *et al.*, many genes encoding cardiac structural proteins are expressed less in hiPSC-CMs than in adult CMs. Furthermore, most calcium handling protein encoding genes included to the study were expressed less, while some were expressed similarly, or more (Rao et al. 2013).

According to Bedada *et al.*, many of the potential maturation markers are susceptible to change and can revert to fetal state due to stress. These include especially genes encoding contractile proteins and ion channels (Bedada, Wheelwright & Metzger 2016). As maturation markers, Bedada *et al.* and Denning *et al.* suggested TNNI1, TNNI2 and TNNI3, since their expression is not affected by stress (Bedada, Wheelwright & Metzger 2016; Denning et al. 2016). In terminally differentiated CMs, the expressed genes can be classified into genes encoding structural proteins, major ion channels, proteins related to calcium handling and genes affecting the metabolism of the CMs (Karakikes et al. 2015). Table 2.1 presents genes characteristic to CM differentiation and terminally differentiated CMs and shows whether they are up- or downregulated in hiPSC-CMs compared to adult CMs.

Table 2. 1 *Genes characteristic to cardiomyocytes and their expression in hiPSC-CMs compared to adult CMs (-: no difference in expression, ↑: upregulated, ↓: downregulated).*

	Type	Gene name	Gene abbreviation	Expression in hiPSC-CMs compared to adult CMs	Reference
During differentiation (expression increased)	*Mesoderm formation*	T-brachyury	BRY	-	(Karakikes et al. 2015)
		ISL LIM homeobox 1	ISL1	-	
		kinase insert domain receptor	KDR	-	
		mesoderm posterior bHLH transcription factor	MESP1	-	
		mix paired-like homeobox	MIXL1	-	
	Cardiac specific progenitors	GATA binding protein 4	GATA4	-	
		heart and neural crest derivatives expressed 1 and 2	HAND-1, -2	-	
		myocyte enhancer factor 2C	MEF2C	-	
		NK2 homeobox 5	NKX2.5	-	
		T-box 5	TBX5	-	
Terminally differentiated CMs	*Structural proteins*	caveolin 3	CAV3	↓	(Rao et al. 2013)
		connexin 43	Cx43	*	
		myosin regulatory light chain 2	MYL2	↓	(Bedada, Wheelwright & Metzger 2016)
		myosin regulatory light chain 7	MYL7	↑	
		myosin regulatory light chain 9	MYL9	*	
		myosin heavy chain 6	MYH6	↓	(Lundy et al. 2013; Rao et al. 2013)
		myosin heavy chain 7	MYH7	↓	
		slow skeletal type troponin I1	TNNI1	*	
		fast skeletal type troponin I2	TNNI2	↑	(Bedada, Wheelwright & Metzger 2016)
		cardiac type troponin I3	TNNI3	↓	
		cardiac type troponin T2	TNNT2	↓	(Rao et al. 2013)
		slow skeletal and cardiac type troponin C1	TNNC1	*	
	Ion channels	voltage-dependent L-type calcium channel subunits alpha 1C	CACNA1C	-	(Rao et al. 2013)
		voltage-dependent L-type calcium channel subunits alpha 1D	CACNA1D	*	
		hyperpolarization activated cyclic nucleotide gated potassium channel 4	HCN4	*	
		potassium voltage-gated channel subfamily D member 3	KCND3	↓	
		potassium voltage-gated channel subfamily H member 2	KCNH2	*	
		potassium voltage-gated channel subfamily Q member 1	KCNQ1	*	
		sodium voltage-gated channel alpha subunit 5	SCN5A	*	
	Calcium handling	sarco-endoplasmic reticulum Ca^{2+} ATPase	ATP2A2	↓	(Lundy et al. 2013; Rao et al. 2013)
		calreticulin	CALR	↓	
		calsequestrin	CASQ2	↓	(Rao et al. 2013)
		inositol triphosphate receptor	IP3R	↓	
		junctophilin	JPH2	↑	
		sodium calcium exchanger	NCX	-	
		phospholamban	PLN	↑	
		ryanodine receptor 2	RYR2	↓	
		triadin	TRDN	↓	
	Metabolism	mitochondrial complexes I-V	-	*	(Karakikes et al. 2015)
		protein kinase AMP-activated non-catalytic subunit gamma 1 and 2	PRKAG-1, -2	*	
		superoxide dismutase 1	SOD1	*	

* Information not available

2.6.2 Molecular maturation of hiPSC-derived cardiomyocytes

For applications in disease modeling, it is crucial that the hiPSC-CMs express disease associated alleles faithfully (Karakikes et al. 2015). Methods to improve hiPSC-CM maturation often affect the molecular maturity of the cells, meaning that their gene expression and thus protein expression is altered. Lundy *et al.* studied the effect of prolonged hiPSC-CM culture to the maturity of the cells and in addition to structural and functional improvement in the maturity, the gene expression of the cells cultured for over 80 days resembled more that of adult heart. MYH7 and MYH6 as well as ATP2A2 expression levels increased to levels of adult heart. Increases were also observed in genes that are not expressed as excessively in adult heart, such as HCN4 and Cx43. (Lundy et al. 2013)

Han *et al.* discovered that culturing hiPSC-CMs on aligned fibers improves the molecular maturation of the cells, who showed increased expression of structural protein encoding genes TNNT2, MYH6, MYL7 and certain ion channel encoding genes (Han et al. 2016). Khan *et al.* showed that hiPSC-CMs cultured on nanofiber patches and standard cell culture plates both had increased Cx43 and slow skeletal and cardiac type troponin C1 (TNNC1) expression. No significant difference was observed in expressions of alpha actin or TNNI3 (Khan et al. 2015). On the other hand, Rao *et al.* studied the effect of microgrooved culture substrates on maturation of hiPSC-CMs and determined that the cells grown on the structured and non-structured culture substrates have similar gene expression and that the topographical cues did not affect the molecular maturation of hiPSC-CMs (Rao et al. 2013).

Chun *et al.* studied ECM mediated maturation of hiPSC-CMs with combinatorial polymer matrices and investigated the expression of MYL2 and TNNI3 as maturation markers. The cells cultured on the polymer matrices showed increased MYL2 and TNNI3 expression indicating more mature molecular phenotype (Chun et al. 2015). Herron *et al.* studied ECM mediated hiPSC-CM maturation on Matrigel coated PDMS coverslips and observed higher expression of SCN5A and Cx43 (Herron et al. 2016). The results suggested that ECM mediated maturation affects also the molecular maturation of hiPSC-CMs.

Pneumatic cell stretching system has been studied by Kreutzer *et al.* as a method to differentiate and maturate hiPSC-CMs. The cells were differentiated and cultured under mechanical stress and it was determined that the stretching did not have a major effect on the differentiation and expression of MYH6, MYH7, Cx43 and TNNI3 genes of the cells (Kreutzer et al. 2014). However, Ruan *et al.* determined that mechanical stress and electrical stimulation together increased the expression of genes related to encoding calcium handling proteins, such as ATP2A2 and RYR2, indicating more mature phenotype (Ruan et al. 2016).

2.6.3 Assessing protein expression of hiPSC-derived cardiomyocytes

To be able to assess the morphology, structural maturity and protein expression of hiPSC-CMs, the structural proteins should be seen and imaged. A typical method for cell structure imaging is staining the structures of interest with specific dyes and imaging them with cameras attached to optical microscopes. Staining of the structure of interest can be based on different properties of the structure, such as basic or acidic properties or immunological properties (Veuthey, Herrera & Dodero 2014). One method for staining is double immunofluorescence staining utilizing the immunological properties of the cells and cell structures. The cells are exposed to antibody molecules specific for a certain target molecule of the cell structure. The primary antibody has an immunoglobulin molecule attached to it and the interaction between the antibodies and the cells is detected by incubating the sample with a secondary antibody specific for immunoglobulin molecules of the primary antibody. The fluorophore producing a visible signal during excitation is attached to the secondary antibody. The results are observed with a fluorescence microscope (Donaldson 2015).

Fluorescence means spontaneous emission of a photon from a molecule when an electron returns to its ground state from a higher energy state. Light energy is absorbed by the molecule and can cause an electron in the outermost low energy orbitals to move into higher energy orbital. As the electron returns to its original orbital, it emits a photon on a longer wavelength than the light absorbed by the molecule and thus distinguishable from the light entering the molecule. This phenomenon can be utilized in imaging cells, since optical contrast achieved by more traditional methods, such as light scattering, absorption or reflection, are not always sufficient enough for seeing cellular structures in detail. (Lavrentovich 2012)

Images acquired from wide-field fluorescence microscopes are good quality if the samples are relatively thin. For thicker samples, the images become blurred, since the excitation light illuminates all the regions of the sample along the optical path and causes fluorescence in all the regions below and above the focus plane (Lavrentovich 2012). Confocal fluorescence microscopy provides three-dimensional (3D) optical resolution by blocking the out-of-focus signal (Lavrentovich 2012; Mueller 2005, pp. 1). These properties make it a very good method to study structural changes occurring in CMs during developmental and pathological processes. CMs undergo structural remodeling as a response to changes in their environment as well as due to pathological changes. Especially the contractile components as well as size-related changes are readily detectable with confocal fluorescence microscopy. (Price et al. 2014)

Proteins typically stained of CMs include troponin T, myosin binding protein C, alpha-actinin, connexin 43, myosin light chain 2a and myosin light chain 2v. Cardiac troponin

T is encoded by TNNT2 gene, and has an important role in fixation of the troponin complex on the actin filament (Katrukha 2013). MyBPC affects the interactions between myosin and actin and is a key regulator of muscle contraction. Staining MyBPC makes the arcomere structure of the CMs visible (Van Dijk, Bezold & Harris 2014), allowing quantification of sarcomere length and alignment. Alpha-actinin is an actin binding protein localized at the Z-disk in cardiac muscle cells and functions as a stabilizer of the muscle contractile apparatus (Sjöblom, Salmazo & Djinović-Carugo 2008). Connexin 43 is the most abundant gap junction forming protein in CMs (Sarantitis et al. 2012). Myosin light chain isoforms 2a and 2v are expressed in atrial and ventricular CMs, respectively (Sheikh, Lyon & Chen 2015). Thus, these can be used in determining the subtype of the CMs.

The out-of-focus signal is blocked in confocal fluorescence microscopy with a pinhole made of opaque material placed in front of the light detector. Thus, only the signal from the level of focus is detected resulting in sharp images (Lavrentovich 2012; Mueller 2005, pp. 1). Confocal fluorescence microscopy can be based either on reflection or transmission of the light from the sample. There are several different modes utilizing different methods in blocking the out-of-focus signal. These include confocal laser scanning microscopy, confocal fluorescence microscopy with Nipkow disk, fluorescence confocal polarizing microscopy and multiphoton microscopy (Lavrentovich 2012). Figure 2.9 shows the principle of removing the out-of-focus fluorescence signal.

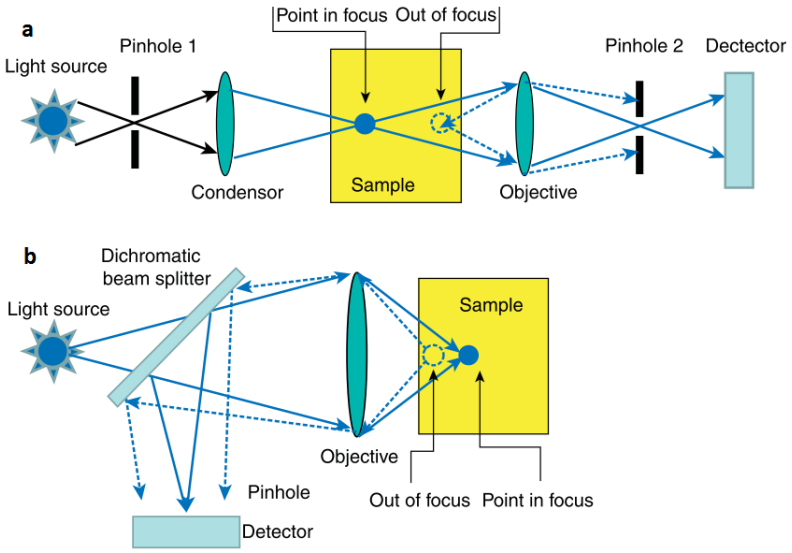

Figure 2. 8 *Principle of confocal fluorescence microscopy, adapted from (Lavrentovich 2012). Point in the plane of focus is detected by the detector, while point out of focus is blocked by the pinhole made of opaque material. Confocal fluorescence microscopy can be based either on a) transmission or b) reflection of the light from the smple.*

In scanning laser confocal microscopy, the illumination and the image are achieved by scanning one or more laser beams across the plane of focus of the sample. The reflected or transmitted light is then detected by a photomultiplier behind the pinhole. 3D image

production is possible by scanning one plane of focus after another until the volume of interest is scanned (Lavrentovich 2012; Paddock & Eliceiri 2014). Advantages of this method include versatility in applications it can be used in, production of high quality images as well as user-friendliness (Paddock & Eliceiri 2014). On the other hand, it is a relatively slow imaging method, especially with thicker objects of interest (Lavrentovich 2012).

Confocal fluorescence microscopy with Nipkow disk, or spinning-disk confocal microscopy, is the most popular of the different confocal fluorescence microscope modes and used especially in live-cell imaging. In spinning-disk confocal microscopy, a disk with regularly spaced pinholes arranged in Archimedean spiral is placed at one of the intermediate image planes of the microscope. The image of the in-focus sample is generated when the illuminated array of pinholes is repeatedly scanned across the sample at sufficiently high rate (Oreopoulos, Berman & Browne 2014). An advantage of spinning-disk confocal microscopy over laser scanning confocal microscopy is that imaging rate is 10-100 times faster (Lavrentovich 2012; Oreopoulos, Berman & Browne 2014). Also, photo bleaching is significantly lower in spinning-disk confocal microscopy allowing live cells to be imaged for longer periods of time with lower risk of phototoxic degradation. Disadvantages include pinhole cross talk effect creating a noticeable hazy background signal and the lack of scan zoom function for altering the sampling rate of the digital images (Oreopoulos, Berman & Browne 2014).

Fluorescence confocal polarizing microscopy combines the benefits of polarizing microscopy and confocal fluorescence microscopy by adding polarizers to a confocal fluorescence microscope. In addition, the sample must be doped with anisometric fluorescent molecular markers. This method allows 3D imaging of orientational order and director patterns of the sample and is capable of detecting very small fluctuations in the director field (Lavrentovich 2012). It can be utilized for example in imaging enzymatic activity of cells (Bigelow 2005, pp. 138).

Multiphoton microscopy overcomes a couple of shortcomings related to the conventional confocal fluorescence microscopy. The shortcomings include photo bleaching, photo damaging and additional absorption of light due to the illumination of the sample below and above the plane of focus. In multiphoton microscopy, the used laser is tightly focused and produced average power of irradiation is safe for most soft and hard materials as well as living cells. The light intensity in the regions further away from the plane of focus is low enough not to produce excitation of the fluorescence markers. However, this method has a disadvantage, since the laser sources required are significantly more expensive compared to those utilized in conventional confocal fluorescence microscopes. (Lavrentovich 2012)

3. AIMS OF THE STUDY

It has been shown in multiple studies that hiPSC-CMs grown without any guidance towards a more mature phenotype are closer to CMs of fetal heart rather than adult heart structurally and relative to gene and protein expression and functionality. There have been many approaches to improve hiPSC-CM maturity, including textile culture substrates that successfully induce structural orientation of hiPSC-CMs leading to more mature phenotype. Also, molecular maturation has been observed.

The aims of this study were to determine whether the culturing hiPSC-CMs on gelatin-coated PET textiles affects the molecular and functional maturation states of the cells. In previous studies of the Heart group (Junnila 2016; Mansikkala 2017), hiPSC-CMs grown on PET textiles with different coatings have shown structurally more mature phenotype than their counterparts grown on flat surfaces. In this study, the structural maturation is further evaluated, the focus shifting on molecular maturation and functionality of the hiPSC-CMs grown on PET textiles.

The hypothesis is that in addition to structural maturation, culturing hiPSC-CMs on gelatin-coated PET textiles induces their molecular maturation as well as functionality.

4. MATERIALS AND METHODS

4.1 Materials

The PET textile used was made in Tampere University of Technology (TUT). Structure of the textile was plain weave derivative and color of the textile was blue. The other side of the textile was heat treated to make it flatter and easier for the cells to attach. Fineness of the PET yarns was 78 dtex and each yarn was composed of 24 filaments. There were six warp yarns per reed dent and the warp density of the textile was around 155 yarns per centimeter. The textile was 7 mm wide and was cut to pieces of 8-9 mm in length. Coverslips with 13 mm diameter were used as a control culture substrate. The structure of the PET textile used is shown in figure 4.1.

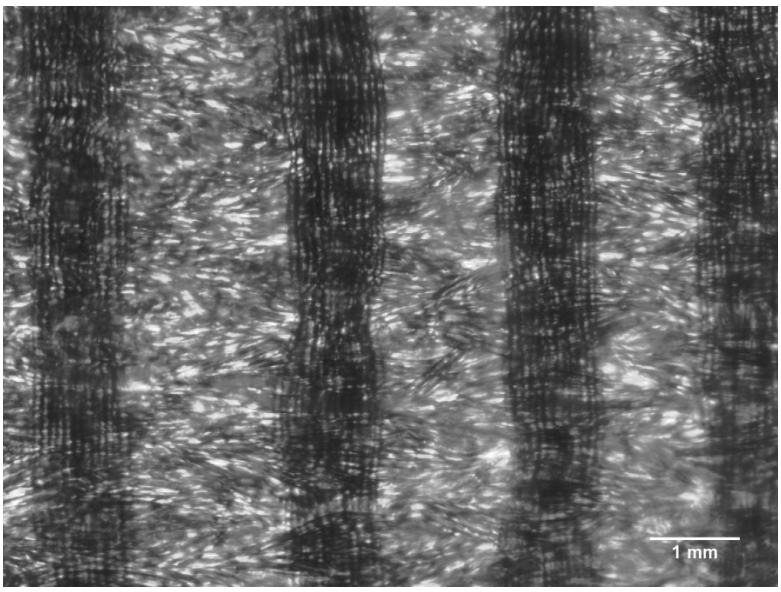

Figure 4. 1 *The PET textile structure. Image taken with Zeiss Axio Vert.A1 microscope and AxioCam MRc5 camera using 5x objective.*

0.1 % gelatin was used as a coating material for PET textiles and coverslips to improve cell attachment to the surfaces. Gelatin powder (gelatin, type A porcine by Sigma-Aldrich) was dissolved in water to make a 0.1 % solution.

4.2 Differentiation of hiPSC-derived cardiomyocytes

The used cell line was UTA04602.WT produced from dermal fibroblasts of a 55-year-old healthy female (Ojala et al. 2012). Several different culture media were used in different phases of the differentiation and culturing of hiPSCs and hiPSC-CMs and they are listed in tables 4.1-4.3. Small molecule differentiation was used in differentiating the hiPSCs into CMs (Vuorenpää et al. 2017).

Table 4. 1 *mTeSR1 medium.*

Volume	Ingredient
400 ml	mTeSR1 basal medium (STEMCELL Technologies)
100 ml	5x Supplement (STEMCELL Technologies)
2.5 ml	Penicillin/Streptomycin (Lonza, Biowhittaker)

Table 4. 2 *Insulin-free RPMI/B27 medium.*

Volume	Ingredient
48.75 ml	RPMI Medium 1640 (1x) + Glutamax (Thermo Fisher Scientific, Gibco)
1 ml	B27 – insulin (50x) (Thermo Fisher Scientific, Gibco)
0.25 ml	Penicillin/Streptomycin (Lonza, Biowhittaker)

Table 4. 3 *RPMI/B27 medium.*

Volume	Ingredient
48.75 ml	RPMI Medium 1640 (1x) + Glutamax (Thermo Fisher Scientific, Gibco)
1 ml	B27 (50x) (Thermo Fisher Scientific, Gibco)
0.25 ml	Penicillin/Streptomycin (Lonza, Biowhittaker)

The frozen UTA04602.WT hiPSCs were thawed, suspended to mTeSR1 medium and plated on a Geltrex-coated 6-well plate. Medium was changed for the cells three times a week by removing half of the old mTeSR1 medium and adding the same amount of fresh medium. After one week the cell monolayer was confluent and one well was chosen and passaged to a new Geltrex-coated 6-well plate. The coating was done by melting and diluting 120 µl of Geltrex (Thermo Fisher Scientific, Gibco) into 12 ml of DMEM/F-12 (1:1) (1x) (Thermo Fisher Scientific, Gibco) medium and adding 2 ml of this mixture to each well of the 6-well plate. The 6-well plate was incubated at 37 °C for an hour, after which the extra Geltrex was aspirated and 3.5 ml of mTeSR1 medium was added to each well. The chosen well was washed with 1xPBS and incubated with Versene (Thermo Fisher Scientific, Gibco) at 37 °C until the monolayer started to detach. The Versene was aspirated and the cells were suspended to 3 ml of mTeSR1 medium. 0.5 ml of the cell suspension was added to each well. The medium was changed three times a week by removing 2 ml of old medium and adding 2 ml of fresh medium.

A week after passaging the cells, the hiPSC monolayer was confluent and the cells were divided into two Geltrex-coated 12-well plates. mTeSR1 medium was aspirated from three wells of the 6-well plate and 1 ml Versene was added to the wells. Cells were incubated in Versene for 4-10 minutes in 37 °C so that the cells started to detach. During incubation, 2 ml of mTeSR1 medium was added to each well of the 12-well plate. Versene was aspirated and 2 ml of mTeSR1 medium was added to the three wells of the 6-well plate. Cells were suspended to the medium and 0.5 ml of the suspension was added to each well of the 12-well plate. This was repeated for the remaining three wells of the 6-well plate so that another 12-well plate of cells was acquired. 1 ml of mTeSR1 medium was changed per well each day until the culture was confluent after four to five days.

Differentiation into CMs was started after the culture was 100 % confluent and the differentiation starting day is referred to as day 0. mTeSR1 medium was aspirated and 2 ml of insulin-free RPMI/B27 (RPMI/B27-I) medium containing 8 µM CHIR99021 (Tebubio, BPS Bioscience) was added to each well. After 24 hours of adding CHIR99021, the old medium was aspirated and 2 ml of RPMI/B27-I was added to each well. On day 3, 1 ml of old medium was collected from each well and mixed with 24 ml of fresh RPMI/B27-I medium. 48 µl of 5 mM IWP-4 (Tocris) was mixed with the medium so that final concentration was 5 µM. The rest of the old medium was aspirated from the 12-well plates and 2 ml of IWP-4 containing medium was added to each well. On days 5 and 7, medium was changed so that old medium was aspirated and 2 ml of fresh RPMI/B27-I medium was added to each well. From day 10 forward, medium was changed three times a week by removing 1 ml of the old medium and adding 1 ml of RPMI/B27 medium to each well.

4.3 Dissociation, separation and plating of hiPSC-derived cardiomyocytes

4.3.1 MACS protocol for cell dissociation and separation

For cell dissociation and separation, 20 % EB medium and MACS Buffer were used and the reagents in the solutions are listed in tables 4.4 and 4.5, respectively. Figure 4.2 presents the outline of the MACS protocol.

Table 4. 4 *20 % EB medium.*

Volume	Ingredient
38.75 ml	KO-DMEM (Thermo Fisher Scientific, Gibco)
10 ml	FBS (Biosera)
0.5 ml	NEAA (Lonza, Biowhittaker)
0.5 ml	GlutaMAX – I (100x) (Thermo Fisher Scientific, Gibco)
0.25 ml	Penicillin/Streptomycin (Lonza, Biowhittaker)

Table 4. 5 *MACS Buffer.*

Amount	Ingredient
47.1 ml	1xPBS (diluted from 10xDPBS from Lonza, Biowhittaker)
0.0370 g	EDTA (Sigma)
2.5 ml	10 % BSA in PBS (BSA powder from Sigma-Aldrich, Fluka dissolved in 1xPBS)
pH of the buffer was balanced to 7.0-7.5 with natrium hydroxide	

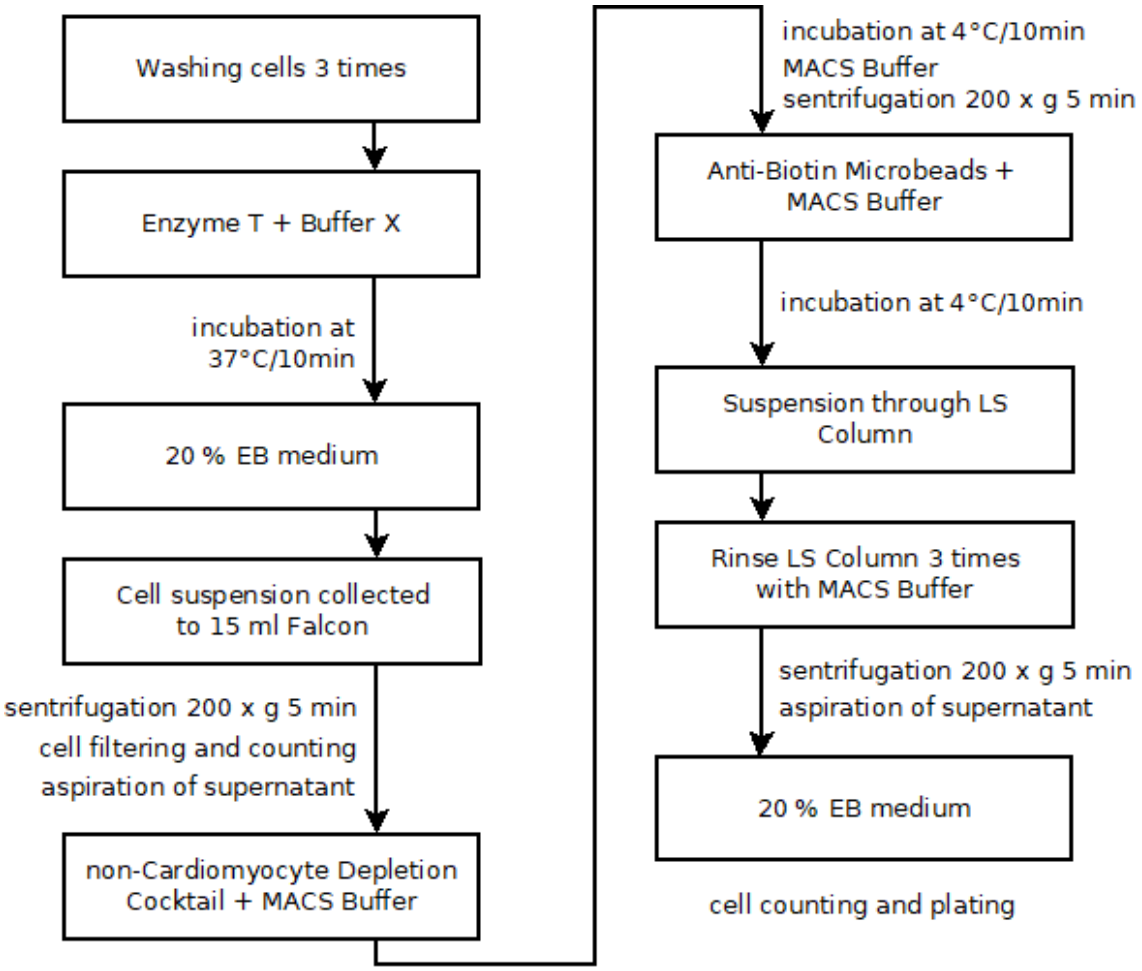

Figure 4. 2 *Outline of the MACS protocol.*

On day 21-27 after starting the differentiation, the cells were dissociated and CMs were separated from the other cell types using MACS. The cells were dissociated with Multi Tissue Dissection Kit 3 (Miltenyi Biotech), which contained Enzyme T and Buffer X. Instructions provided by the kit were followed. The chosen wells from the 12-well plate were each washed three times with 1 ml of 1xPBS. 40 µl of Enzyme T and 360 µl Buffer X were added to each well and incubated for 10 minutes in 37 °C. After incubation, 400 µl of 20 % EB medium was added to each well and the cells were suspended into it and the suspension from each well was collected into 15 ml Falcon tube. The cell suspension was filtered to remove large cell aggregates. The cell number was calculated with a hemocytometer to ensure that the number of cells was smaller than 5 million and a single reaction volume could be used during separation protocol. If the number of cells was higher, the cells were divided into multiple 15 ml Falcon tubes so that the cell number did not exceed 5 million. The following protocol was done to each tube separately.

MACS Buffer and PSC-Derived Cardiomyocyte Isolation Kit, human (Miltenyi Biotech) containing non-Cardiomyocyte Depletion Cocktail and Anti-Biotin MicroBeads, and LS Columns were used to separate CMs from the other cell types. Instructions provided by the kit were followed. At first, the Falcon tubes containing the cells were centrifuged at 4

°C 200 x g for 5 minutes, after which the supernatant was aspirated. 20 µl of non-Cardiomyocyte Depletion Cocktail and 80 µl of MACS Buffer were added into each tube on the cell pellet and the cells were suspended to the mixture and incubated at 4 °C for 10 minutes. 1 ml MACS Buffer was added to the suspension and the cells were centrifuged again at 4 °C 200 x g for 5 minutes. The supernatant was aspirated and 20 µl of Anti-Biotin MicroBeads and 80 µl of MACS Buffer were added into each tube on the cell pellet and the cells were suspended to it and incubated at 4 °C for 10 minutes.

During incubation, LS Column was attached to MidiMACS Separator secured by MACS MultiStand. LS Column contains a matrix, to which the labeled cells attach when placed in a permanent magnet, in this case MidiMACS Separator. The column was prepared by rinsing it with 3 ml of MACS Buffer. After the incubation, the cell suspension was added to the column and the flowthrough was collected to 15 ml Falcon tube. The column was rinsed three times with 3 ml of MACS Buffer and the flowthrough was collected to the same Falcon tube. This tube now contained the hiPSC-CMs. If multiple Falcon tubes were used due to large number of cells, this step was repeated with new LS Column for each set of cells. Thus, samples processed later, were incubated in Anti-Biotin MicroBead solution for a longer period of time.

The Falcon tubes containing the hiPSC-CMs were centrifuged at 4 °C 200 x g for 5 minutes and the supernatant was aspirated. The cells were suspended to 1-2 ml of 20% EB medium depending on the number of cells expected from the separation. The number of cells was calculated again with hemocytometer and the cells were suspended to 20% EB medium so that the cell concentration would be 175 000 cells in 600 µl of medium. After this, the cells were ready for plating.

4.3.2 Plating and culturing of hiPSC-derived cardiomyocytes

The cells were plated on 4-well plates with PET textile pieces on two wells and coverslips on two wells. The wells and the PETs and coverslips in them were coated with 0.1 % gelatin so that 500 µl of gelatin was added to the wells and incubated in room temperature for at least an hour. The extra gelatin was aspirated just prior to cell plating. The hiPSC-CMs were plated on the wells by adding the cell suspension acquired from the separation on the PETs and coverslips. 600 µl of the cell suspension was pipetted slowly and directly on the PETs to ensure that as many cells would attach to it as possible. To the wells with coverslips, 600 µl of the suspension was pipetted against the well wall near the bottom so that the cells would spread evenly. Figure 4.3 shows the set up.

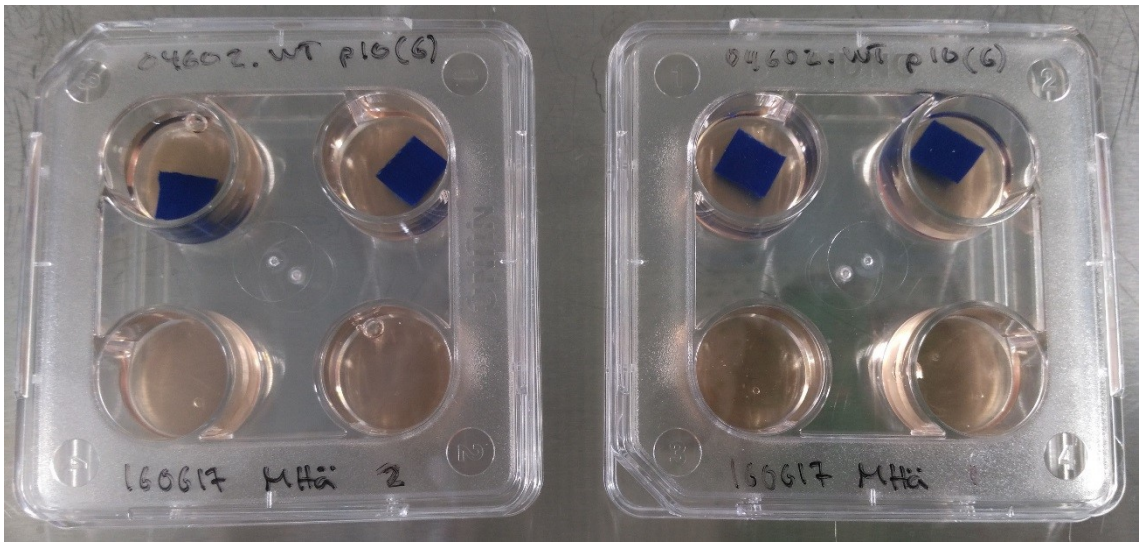

Figure 4. 3 *Set up for culturing hiPSC-CMs on PET textiles and coverslips.*

Day of the cell plating was considered as day 0. 20 % EB medium was changed two times a week so that 400 µl of the old medium was removed and 400 µl of fresh medium was added. On day 11 RNA extraction and immunofluorescence staining were performed. In gene expression studies of hiPSC-CMs, also time control was used. hiPSC-CMs plated on coverslips were cultured for one day, after which they were taken for RNA extraction. Calcium imaging was done on day 12 and the medium was changed the previous day by removing 400 µl old medium and adding 400 µl fresh medium.

4.4 Immunofluorescence staining and imaging

Double fluorescence protocol was followed in immunofluorescence staining of the samples (Ojala et al. 2012). The PET textiles and coverslips in the 4-well plate were moved to another 4-well plate and contents of both 4-well plates were stained. The culture plate was stained to determine how much cells slid through the textiles on the bottom of the well. The protocol can be divided into fixing the cells, blocking non-specific staining, primary antibody incubation and secondary antibody incubation. Figure 4.4 presents the outline of the protocol.

The samples were washed two times with 1xPBS for 5 minutes. After this, they were fixed with 4 % paraformaldehyde solution for 20 minutes and washed again two times with 1xPBS for 5 minutes. The blocking was done by incubating the samples in blocking solution containing 10 % normal donkey serum (NDS) (Biowest), 0.1 % TritonX-100 (Sigma-Aldrich) and 1 % bovine serum albumin (BSA) (Sigma-Aldrich, Fluka) in 1xPBS for 45 minutes. During incubation, mixture of primaries containing 1 % NDS, 0.1 % TritonX-100 and 1 % BSA in 1xPBS and the primary antibodies was prepared. The primary antibodies used were goat polyclonal IgG Troponin T (Abcam) diluted 1:1000 and mouse monoclonal IgG MyBPC3 (Santa Cruz Biotechnology) diluted 1:400 to the basal solution.

After incubation, mixture of primaries was added to each well and incubated at 4 °C overnight.

Next day, the samples were washed three times with 1 % BSA in 1xPBS for 7 minutes. Mixture of secondaries containing 1 % BSA in 1xPBS and the secondary antibodies was prepared. The used secondary antibodies were donkey anti-goat Alexa fluor 568 (Thermo Fisher Scientific) and donkey anti-mouse Alexa fluor 488 (Thermo Fisher Scientific), both diluted 1:800 to the basal solution. Mixture of secondaries was added to each well and incubated for an hour. After incubation, the samples were washed three times for 5 minutes with 1xPBS and two times for 5 minutes with phosphate buffer working solution. PETs and coverslips were transferred to microscope glasses and mounted with Vectashield mounting medium with DAPI (Vector Laboratories). Vectashield was added also to each well of the stained culture plate and the wells were covered with coverslips of 13 mm in diameter. The samples were stored light protected at 4 °C.

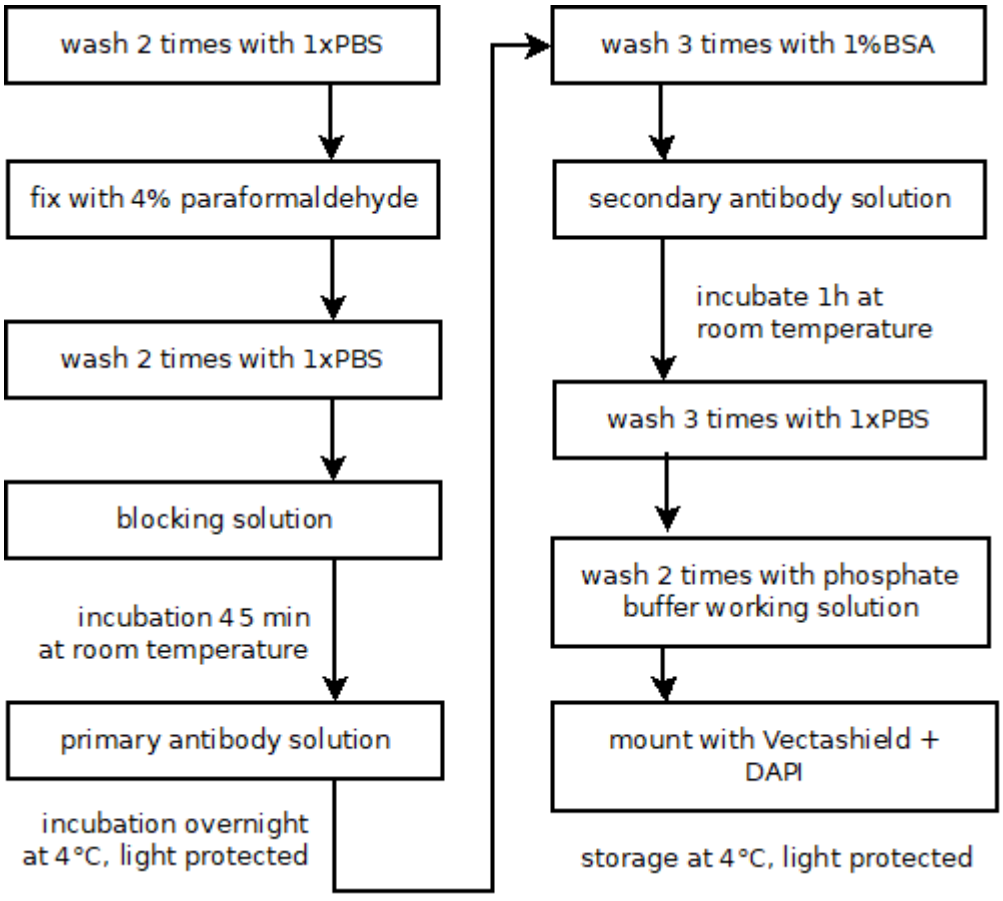

Figure 4. 4 *Outline of the double fluorescence immunostaining protocol.*

The samples were imaged with Nikon A1R+ Laser Scanning Confocal Microscope using Nikon Apo 60x 1.40NA oil objective to get high quality detailed images of the cell structures. Myofibril orientation and sarcomere length of the samples were determined from images taken with Zeiss Axio Imager.M2 with ApoTome.2 and AxioCamHRm3 camera using Zeiss EC Plan-Neofluar 40x 1.30NA oil objective.

4.5 RNA extraction and PCR

Two methods were used to extract RNA from the cells. Straight RNA extraction with Total RNA Purification Plus Micro Kit (Norgen Biotek Corporation) and cell lysing with CellsDirect One-Step qRT-PCR Kit (Invitrogen) where RNA was not actually extracted, but reverse transcription was performed to the cell lysis after degrading genomic DNA. RNA extraction with the Total RNA Purification Plus Micro Kit yielded small concentrations of RNA and the reverse transcription into complementary DNA (cDNA) and PCR from the cDNA was unsuccessful, which is why CellsDirect One-Step qRT-PCR Kit was chosen as the primary method for the gene expression studies.

The protocol for CellsDirect One-Step qRT-PCR Kit is divided into three parts, including lysing the cells, reverse transcription-specific target amplification (RT-STA) and quantitative PCR (qPCR). RT-STA is typically used for single-cell PCR, but was used in this case to amplify the target cDNA for the Fluidigm Integrated Fluidic Circuit for comprehensive gene expression evaluation (Ojala et al. 2016). Figure 4.5 presents the outline of the protocol. All the used solutions were provided by the kit, unless mentioned otherwise. Instructions provided by the kit were followed.

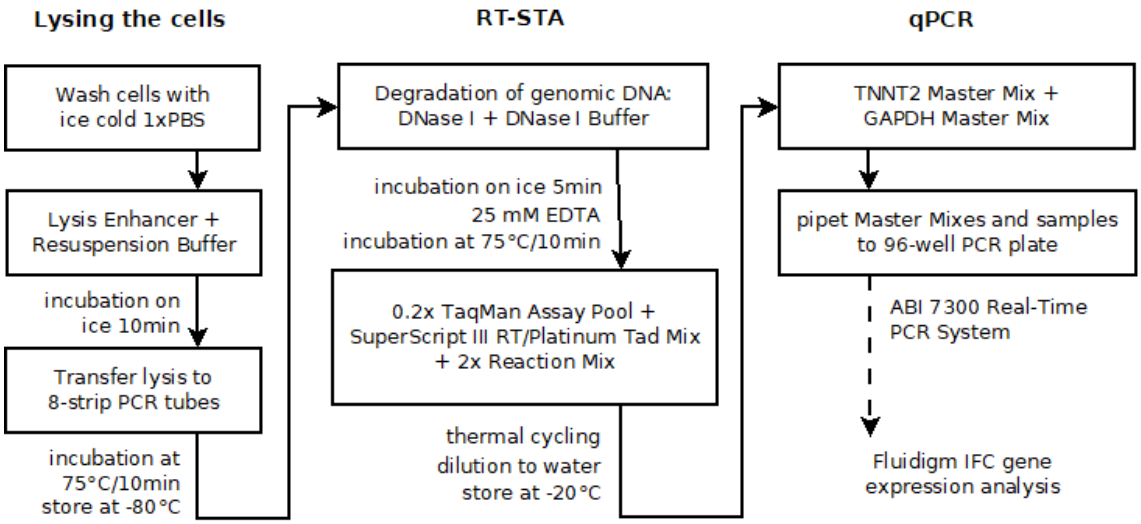

Figure 4. 5 *Outline of the qPCR protocol.*

The cells were lysed with Lysis Solution Master Mix containing 1:10 Lysis Enhancer and Resuspension Buffer. The cells grown on PETs and coverslips were washed with ice cold 1xPBS so that the 4-well plate the cells were in was also on ice. 50 µl of Lysis Solution Master Mix was added to each well and incubated on ice for 10 minutes. The solution was pipetted to the middle of the wells a couple of times during incubation. After incubation, the cells were scraped from PETs and coverslips with pipette tip and the 50 µl of the lysis solution was divided into two tubes of 8 strip PCR tubes so that each contained 25 µl of the solution. The 8 strip PCR tubes were incubated at 75 °C for 10 minutes. The lysis was stored at -80 °C if the next step could not be performed right away.

RT-STA was performed for 7 samples, including samples from one 4-well plate (2 PET and 2 coverslip samples), total human heart RNA, water control and –RT sample, where one of the coverslip samples was used. In –RT sample, the polymerase containing reagent is left out during PCR reaction. First, the genomic DNA was degraded with Master Mix I containing 40 µl of DNase I, Amplification Grade (1 U/µl) and 12.8 µl of 10x DNase I Buffer. 10 µl of the samples mentioned were added to 8 strip PCR tubes and in case of total human heart RNA sample, 1 µl of the sample diluted to 9 µl of water was used. 6.6 µl of Master Mix I was added to each sample and incubated for 5 minutes. After this, 4 µl of 25 mM EDTA was added to each sample and incubated at 75 °C for 10 minutes.

0.2x TaqMan Assay Pool was prepared by adding 1 µl of 35 different 20x TaqMan Gene Expression Assays (Thermo Fisher Scientific) to 65 µl of DNA Suspension Buffer (Teknova). The 20x TaqMan Gene Expression Assays contained forward and reverse primers for different genes, which are listed and categorized based on their function in table 4.6.

7 µl of Master Mix II containing 20 µl 0.2x TaqMan Assay Pool, 1.6 µl SuperScript III RT/Platinum Tad Mix and 34.4 µl 2x Reaction Mix was added to 6 tubes of a new 8 strip PCR tubes and 7 µl of Master Mix II –RT containing 2.5 µl 0.2x TaqMan Assay Pool and 4.5 µl 2x Reaction Mix was added to one tube. 2 µl of Master Mix I treated samples were added to the tubes so that –RT sample was added to the one containing Master Mix II –RT. The 8 strip PCR tubes were loaded to a thermal cycler. Program used for RT-STA is shown in table 4.7. After RT-STA the acquired samples were stored at -20 °C.

To perform the qPCR, the samples from the RT-STA reaction were diluted 1:5 with water. The qPCR analysis for TNNT2 was performed as follows. Two different Master Mixes were made for qPCR reaction, the other containing 13 µl GAPDH 20x TaqMan Assay Pool and the other 13 µl TNNT2 20x TaqMan Assay Pool. In addition, both contained 130 µl TaqMan Gene Expression Master Mix (Thermo Fisher Scientific) and 91 µl water. 9 µl of the GAPDH Master Mix and TNNT2 Master Mix was pipetted each to 24 tubes of a 96-well PCR plate. Each diluted sample was pipetted on three tubes containing GAPDH Master Mix and three tubes containing TNNT2 Master Mix. The 96-well plate was then loaded to ABI 7300 Real-Time PCR System. Program used for qPCR reaction is shown in table 4.8.

The diluted samples were stored at -80 °C for further use in Fluidigm Integrated Fluidic Circuit, which allows quantification of all amplified genes from the samples.

Table 4. 6 *The 35 amplified genes (TaqMan Gene Expression Assays).*

Function	Type	Gene
Sarcomeric genes	Myosin light chain	MYL2, MYL7, MYL9
	Myosin heavy chain	MYH6, MYH7
	Troponin	TNNC1, TNNT2, TNNI3
	Other	ACTN2 (actinin), TTN (titin), MYBPC3 (myosin binding protein), TPM1 (tropomyosin)
Ion channel encoding genes	Potassium	KCNH2, KCNH6, KCND3, KCND10, KCNQ1, HCN4
	Other	SCN5A (sodium), CACNA1C (calcium)
Ion exchanger encoding genes	Sodium-calcium ex-changer	SLC8A1
Calcium handling related genes		RYR2, JPH2, CASQ2, PLN, ATP2A2
Signaling related genes	Hormone	NPPB
	Receptor	ADRB1, ITPR2
	Connexin 43	GJA1
Non-protein coding genes		NPPA-AS1
Housekeeping genes		EEF1A1; EE+, GAPDH, RPLP0, TBP

Table 4. 7 *Thermal cycler program for reverse transcription-specific target amplification.*

Temperature	Time	Cycles
50 °C 95 °C	15 min 2 min	1
95 °C 60 °C	15 s 5 min	18
4 °C	∞	1

Table 4. 8 *Thermal cycler program for qPCR.*

Temperature	Time	Cycles
60 °C 95 °C	2 min 10 min	1
95 °C 60 °C	15 s 1 min	40

4.6 Calcium imaging

Calcium imaging was done with Risto-Pekka Pölönen to compare the functionality of the hiPSC-CMs grown on PET textiles and coverslips.

Calcium imaging is based on the changes in the amount of intracellular calcium during contraction and relaxation of the cells. Before and during contraction, the amount of cytosolic calcium is increased causing the cell to contract, after which the calcium is removed from the cytosol and the cell relaxes (Ross & Pawlina 2016, pp. 334-335). The cells are loaded with cell permeable fluorescent dye, which undergoes large fluorescent enhancement upon binding calcium ions as the amount of intracellular calcium increases. Thus, by measuring the intensity of the fluorescent light, the calcium kinetics of the cells can be evaluated (Gee et al. 2000). As the cells contract, the amount of intracellular calcium increases causing peak in the fluorescent intensity, which decays as the cell relaxes

and the amount of intracellular calcium decreases leading to the decrease of the fluorescent light intensity back to the baseline.

Extracellular solution was prepared by adding the ingredients described in table 4.9 and balancing the pH of the solution between 7.35 and 7.40 with 1 M NaOH. After the solution was ready, the osmolarity of the solution was measured and determined to be 310 mOsm/kg. Also, the osmolarity of the cell culture medium was measured and determined to be 296 mOsm/kg, which was close enough to the extracellular solution not to cause a shock to the cells.

Table 4. 9 *Extracellular solution.*

Ingredient	**Volume**
1 M NaCl	68.5 ml
1 M KCl	2.5 ml
1 M KH_2PO_4	0.22 ml
1 M HEPES	10 ml
1 M $NaHCO_3$	2.1 ml
1 M D-glucose	2.5 ml
1 M $CaCl_2$	1 ml
1 M $MgCl_2$	0.6 ml
1 M Na-pyruvate	0.5 ml
dH_2O	Added until total volume was 500 ml

The live dye was prepared by adding 11.4 µl of 1 mM DMSO (Thermo Fisher Scientific) into an unopened vial containing 50 µg of Fluo 4 AM (Thermo Fisher Scientific) so that the final concentration of the color was 4 µM. Samples were labeled by adding 1 µl Fluo 4 solution to 1 ml of the extracellular solution and putting the sample into the mixture for a half an hour. The imaging was done for the PET textiles and coverslips on which the hiPSC-CMs were grown. The prepared sample was put to an imaging chamber (RC-25, Warner Instruments) and the chamber was put onto a microscope and connected to a perfusion system. The cells were perfused with warm (37 °C) extracellular solution so that the change in temperature would not affect the results as much. The recording was done

with Olympus IX71 microscope using ANDOR iXon+ camera and Olympus UApo 20x 0.75NA air objective and using Live Acquisition software by TILL Photonics. The recordings were 30 seconds long with 20 ms sampling rate.

The response of the hiPSC-CMs to adrenaline was also tested. 5 mM adrenaline stock solution by Sigma-Aldrich was diluted to extracellular solution so that the final adrenaline concentration was 1 µM. The extracellular solution containing adrenaline was connected to the perfusion system, so that it could be easily changed between the pure extracellular solution and the extracellular solution containing adrenaline. When measuring adrenaline response of the cells, first baseline without adrenaline was measured and then adrenaline was let to affect the cells for approximately one minute, after which the adrenaline response of the cells was measured. The adrenaline was washed off for two minutes before making new baseline measurements. The response of only PET samples was tested.

4.7 Analysis

4.7.1 Relative gene expression

Data acquired from qPCR was analyzed using $2^{-\Delta\Delta C_T}$ method for the C_T values (Livak & Schmittgen 2001). GAPDH was used as a housekeeping gene and the amount of TNNT2, was normalized to that. The expression of TNNT2 in hiPSC-CMs grown on PET textiles and coverslips for 11 days was compared to that of hiPSC-CMs grown on coverslips for 1 day. The equation $2^{-\Delta\Delta C_T}$ gives the change in gene expression where $\Delta\Delta C_T$ is defined as following (Livak & Schmittgen 2001).

$$\Delta\Delta C_T = \left(C_{T,TNNT2} - C_{T,GAPDH}\right)_{sample\ CM} - \left(C_{T,TNNT2} - C_{T,GAPDH}\right)_{1d\ coverslip\ CM} \quad (1)$$

Averages of $C_{T,TNNT2}$ and $C_{T,GAPDH}$ of the hiPSC-CMs grown on coverslips for 1 day were used so that the latter part of the equation was constant. The change in gene expression was then calculated for each sample individually and average was taken from each set representing the similar culture conditions.

4.7.2 Cellular orientation and sarcomere length

Cellular orientation and sarcomere length were analyzed from the ApoTome images using CytoSpectre software (Kartasalo et al. 2015). Prior to the analysis, the images were processed with ImageJ software. The images were segmented manually so that the cells in the same image were analyzed separately. Only cells with clear sarcomere structure were included to the analysis. If the signal-to-noise ratio was less than one or the mode wavelength of detailed component (sarcomere length) was less than 1 or higher than 3, the cell was excluded from the results.

CytoSpectre allows quantification of orientation and size distribution cellular structures seen in microscopy images. The software estimates the power spectrum of the image utilizing Fourier transform and computes parameters describing mean orientation and size of target structures based on the spectrum, along with other parameters (Kartasalo et al. 2015). Since cell orientation and sarcomere length were the parameters of interest in this study, circular variance of mixed spectral component, wavelength of detailed spectral component and the ratio of the major to minor axis were the parameters of interest in the analysis.

Circular variance describes cell structure orientation with values from 0 to 1, value 0 indicating perfect structural orientation into a single direction and value 1 indicating that the structures are oriented equally in all directions (Kartasalo et al. 2015). In the case of CMs, the more oriented the sarcomeres are in a single direction, the closer the circular variance would be to 0, while values close to 1 would indicate that the myofibrils are oriented equally to all directions. It is expected that hiPSC-CMs grown on PET textiles would have significantly more oriented sarcomere structure meaning smaller circular variance than hiPSC-CMs grown on coverslips.

Wavelength of the detailed spectral component gives the sarcomere length. Modal wavelength of each cell was used to calculate the average sarcomere length of both CMs grown on PET textiles and CMs grown on coverslips. Modal wavelength gives the most common sarcomere length observed in the cells. Since mature adult CMs are rod-like in shape, also the longitudinal orientation of the cells was studied from the ratio of the major to minor axis of the cells describing the ratio of length to width of the cells.

Circular variance and modal wavelength were determined from the green channel of the fluorescence RGB images, in which the MyBPC3 was stained. Ratio of major to minor axes was determined from the masks created with ImageJ used in the segmentation of the cells. The masks were created manually from the red channel of the fluorescence RGB images, in Troponin T was stained.

4.7.3 Calcium kinetics

The calcium imaging raw data was acquired as fluorescence videos which were converted into numerical data. TILL Photonics Offline Analysis software was used to calculate $\Delta F/F_0$ to normalize differences of the indicator concentration between the cells and to acquire the kinetics data from the videos. Clampfit data analysis module of Axon pCLAMP 10 Electrophysiology Data Acquisition & Analysis Software was used for peak detection. The acquired parameters of interest regarding this study were peak duration, rise time from 10 % to 90 %, decay time from 90 % to 10% and peak frequency.

Peak duration is the time one calcium event takes to rise and decay back to baseline. Rise time from 10 % to 90% describes the amount of time it takes the intracellular calcium to

rise from 10 % of the amplitude maximum to 90 % of the amplitude maximum. Decay time from 90 % to 10 %, on the other hand, describes how long it takes the intracellular calcium to decay from 90 % of the amplitude maximum to 10 % of the amplitude maximum. Finally, peak frequency describes how often the peaks occur, indicating the beating rate of the cells.

4.7.4 Statistical analysis

Statistical analysis regarding gene expression and structural properties was done using Microsoft Excel. Difference in circular variance, mean wavelength, ratio of major to minor axis and the expression of TNNT2 between the hiPSC-CMs grown on coverslips and PET textiles was statistically tested with nonparametric Mann-Whitney U test, since the data did not follow normal distribution. The test was performed using 5 % risk level to see whether there was a statistically relevant difference between the groups or not. The null hypothesis in each case (TNNT2 expression, circular variance, mean wavelength and ratio of major to minor axis) was that there is no difference between the groups and the alterative hypothesis was that there is a difference between the groups regarding these parameters.

Statistical analysis of calcium imaging data was done using SPSS Statistics software. Differences in peak duration, rise time from 10 % to 90 %, decay time from 90 % to 10 % and peak frequency between hiPSC-CMs grown on coverslips and PET textiles was tested with Mann-Whitney U test with 5 % risk level to determine the statistical significance of the results. In addition, the cells were visually categorized as normal or abnormal based on their calcium transient profiles. Only cells classified as normal were included in the statistical analysis. The number of abnormal cells was calculated, and the abnormalities were further classified based on the shape of the calcium peak.

5. RESULTS

Results from relative gene expression, different structural properties and calcium kinetics of hiPSC-CMs grown on PET textiles and coverslips are presented in tables and boxplot graphs to give a thorough understanding of the distribution of the values between different samples. Tables present mean values with standard deviations, while in boxplot graphs, the distribution of the values is better seen compared to table presentation. In the boxplot graphs, the box represents 50 % of the values and the line dividing the box represents the median. The whiskers show minimum and maximum values and x shows the mean value.

5.1 Cellular orientation and sarcomere length

Cellular orientation and sarcomere length of the hiPSC-CMs were evaluated to determine the structural maturation of the cells. The structural properties of the cells were studied using immunocytochemical staining and fluorescence imaging. Stained structures were Troponin T and MyBPC3. DAPI, the nuclear counterstain, was used as well.

Figure 5.1 shows the structural differences between hiPSC-CMs grown on PET textiles and coverslips. As can be seen from the images, hiPSC-CMs grown on PET textiles exhibit relatively rod-like structure and aligned sarcomeres, while hiPSC-CMs grown on coverslips are round or polygonal and exhibit no clear longitudinal axis. In addition, their sarcomeres are less oriented and in many cases circle around the cell edges even though they might be better aligned in the middle of the cell. The sarcomere striations are perpendicular to the myofibril orientation, meaning that horizontal sarcomere striations indicate vertical myofibril alignment.

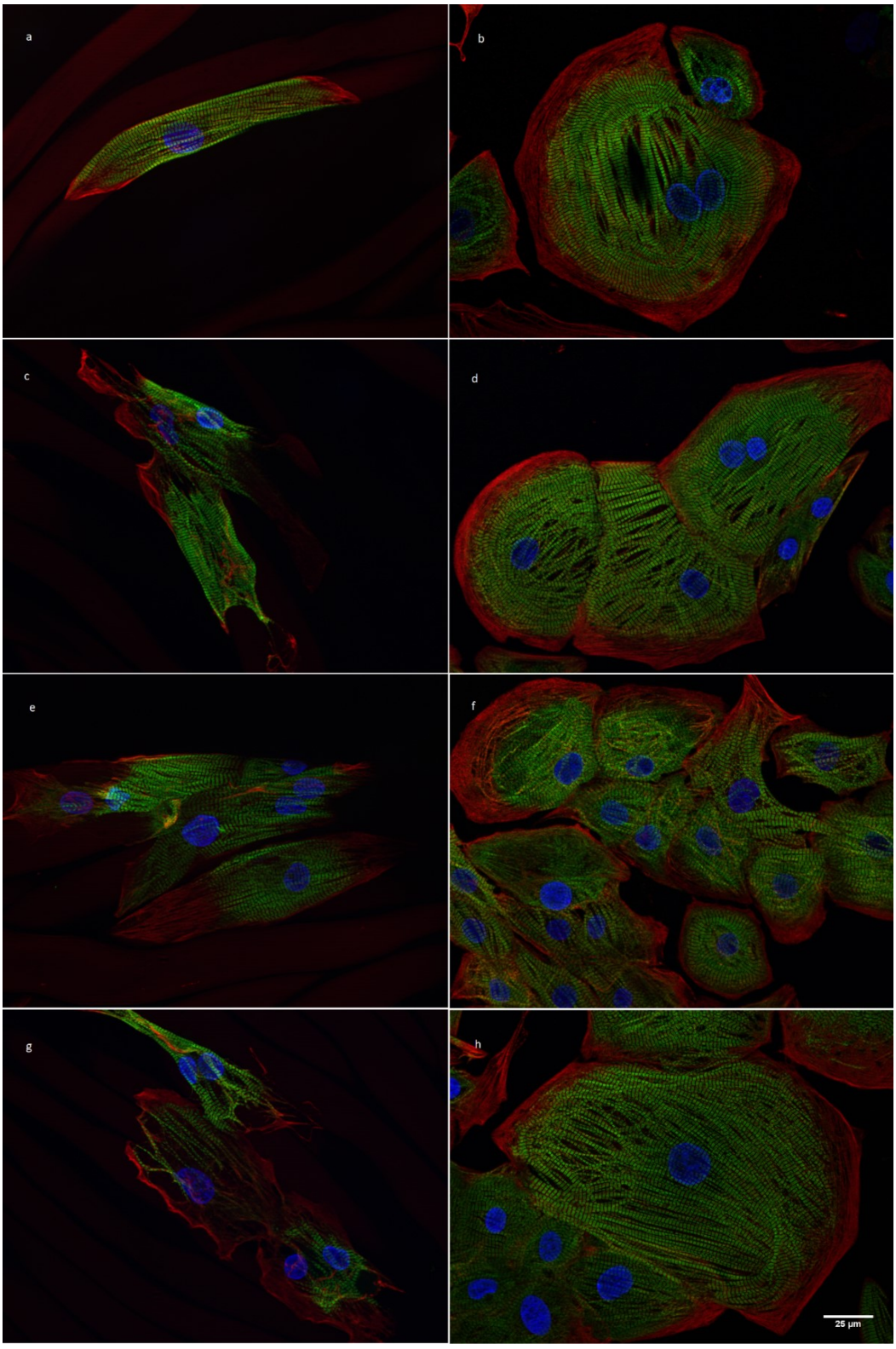

Figure 5. 1 *Images of hiPSC-CMs grown on PET textiles (left) and coverslips (right) stained with Troponin T (red), MyBPC3 (green) and DAPI (blue). Imaged with Zeiss Axio Imager.M2 microscope with ApoTome and AxioCamHRm3 camera using 40x objective. Images demonstrate the alignment of the cells and their sarcomeres (green) according to the textile fibers, while cells cultured on coverslips are round and exhibit no clear sarcomere orientation.*

Figure 5.2 presents the structure of hiPSC-CMs grown on PET textiles in higher detail. The image is taken with confocal laser scanning microscope with 60x objective. The sarcomere structure and alignment are better seen in this image compared to figure 5.2. The image also demonstrates, why Troponin T staining was used to determine cell borders in cell segmenting, since MyBPC3 stained sarcomeres do not fill the whole cell, which would cause relatively large error in cell size and shape in some cases, such as the top side cell of the image.

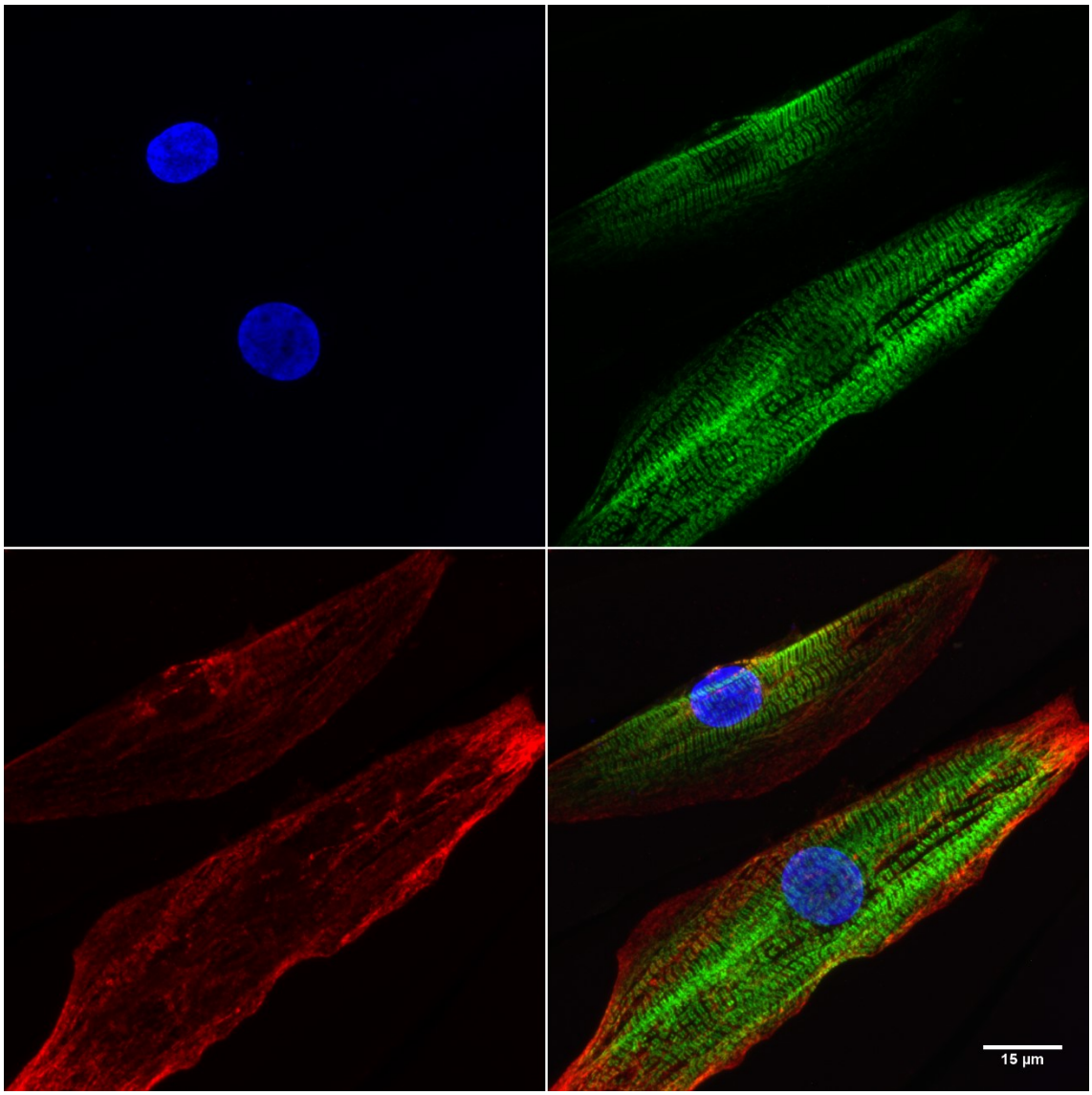

Figure 5. 2 *Image of hiPSC-CM grown on PET textiles stained with Troponin T (red), MyBPC3 (green) and DAPI (blue). Imaged with Nikon N-SIM microscope using 60x objective. The image further demonstrates the structure and alignment of the sarcomeres of hiPSC-CMs grown on PET textiles.*

CytoSpectre software was used to analyze images taken with 40x objective and processed with ImageJ prior to the analysis. If there were multiple cells in the same image, the image was segmented so that each cell was analyzed separately. The parameters acquired from

the analysis included circular variance, mean wavelength and major and minor axes of the cells. Circular variance describes the alignment of the cell and ranges from 0 to 1, zero meaning perfect alignment and one the opposite. Modal wavelength describes the most common sarcomere length of the cell. The ratio of major to minor axis describes the longitudinal alignment of the cell. The average values and standard deviations of circular variance, mean sarcomere length and ratio of major to minor axis are presented in table 5.1, which also shows the number of cells analyzed in both groups. The results are also illustrated in figure 5.3.

Table 5. 1 *Average values and standard deviations of circular variance, modal sarcomere length and ratio of major to minor axis of hiPSC-CMs grown on PET textiles and coverslips.*

Sample	Average circular variance (0-1)	Average modal sarcomere length (µm)	Average ratio of major to minor axis (length/width)	Number of cells
PET	0.611 ± 0.162	1.736 ± 0.187	4.915 ± 2.263	98
coverslip	0.882 ± 0.069	1.749 ± 0.122	1.567 ± 0.455	174

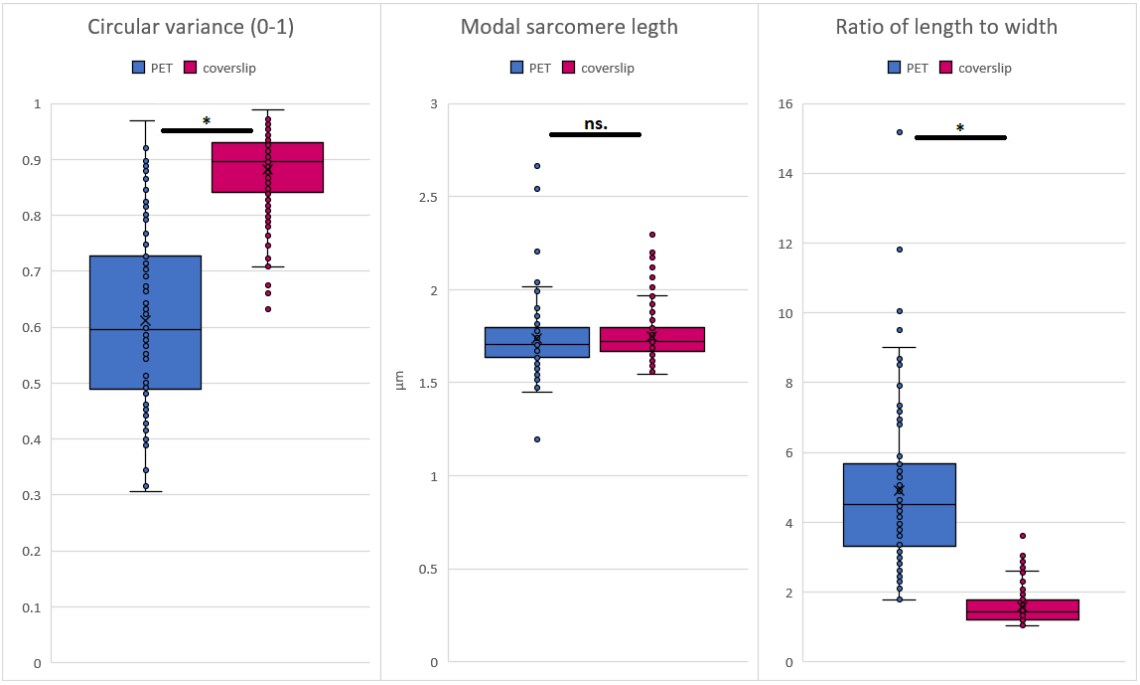

Figure 5. 3 *Circular variance, modal sarcomere length and length to width ratio of hiPSC-CMs grown on PET textiles and coverslips.*

The difference in circular variance between hiPSC-CMs grown on coverslips and PET textiles was statistically significant with 95 % certainty. The average circular variance of

hiPSC-CMs grown on PET textiles was 0.611 with standard deviation of 0.162 while for hiPSC-CMs grown on coverslips it was 0.882 with standard deviation of 0.069. On the other hand, difference in modal sarcomere length (modal wavelength) was not statistically significant with 5 % risk level. The average modal sarcomere length of hiPSC-CMs grown on PET textiles was 1.736 µm with standard deviation of 0.187 µm while for hiPSC-CMs grown on coverslips it was 1.749 µm with standard deviation of 0.122 µm.

The difference in average ratio of major to minor axis between hiPSC-CMs grown on coverslips and PET textiles was statistically significant with 95 % certainty. The average ratio of length to width of hiPSC-CMs grown on PET textiles was 4.915 with standard deviation of 2.263 while for hiPSC-CMs grown on coverslips it was 1.567 with standard deviation of 0.455. This indicates that the cells grown on PET textiles exhibit clearly more rod-like and elongated structure compared to cells grown on coverslips, because the cells have a limited number of directions they can spread to, when cultured on fibers.

5.2 Relative gene expression

Gene expression of TNNT2 was compared between the hiPSC-CMs grown on PET textiles and coverslips was evaluated to determine whether the maturation of the hiPSC-CMs grown on PET textiles is induced also on a molecular level in addition to the structural level. RT-STA was performed to the cell lysis after which the samples were prepared for qPCR. The number of samples was 14 for both hiPSC-CMs grown on PET textiles and coverslips cultured for 11 days and 4 for hiPSC-CMs grown on coverslips for 1 day. One sample included the cells from one piece of PET textile or one coverslip. The samples were from three differentiation batches and there were at least two parallel samples were from one batch. TNNT2 expression was normalized to GAPDH expression and TNNT2 expression was determined using $2^{-\Delta\Delta C_T}$ method.

Average relative TNNT2 expressions and standard deviations of hiPSC-CMs grown on PET textiles and coverslips are presented in table 5.2. The results are also illustrated in figure 5.4.

Table 5. 2 *The average relative TNNT2 expressions of hiPSC-CMs grown on PET textiles and coverslips for 11 days and hiPSC-CMs grown on coverslips for 1 day (time control). Expressions are normalized to GAPDH.*

Sample	Average relative TNNT2 expression	Number of samples
PET (11 days)	6.752 ± 5.438	14
Coverslip (11 days)	2.014 ± 1.391	14
Coverslip (1 day)	1.107 ± 0.544	4

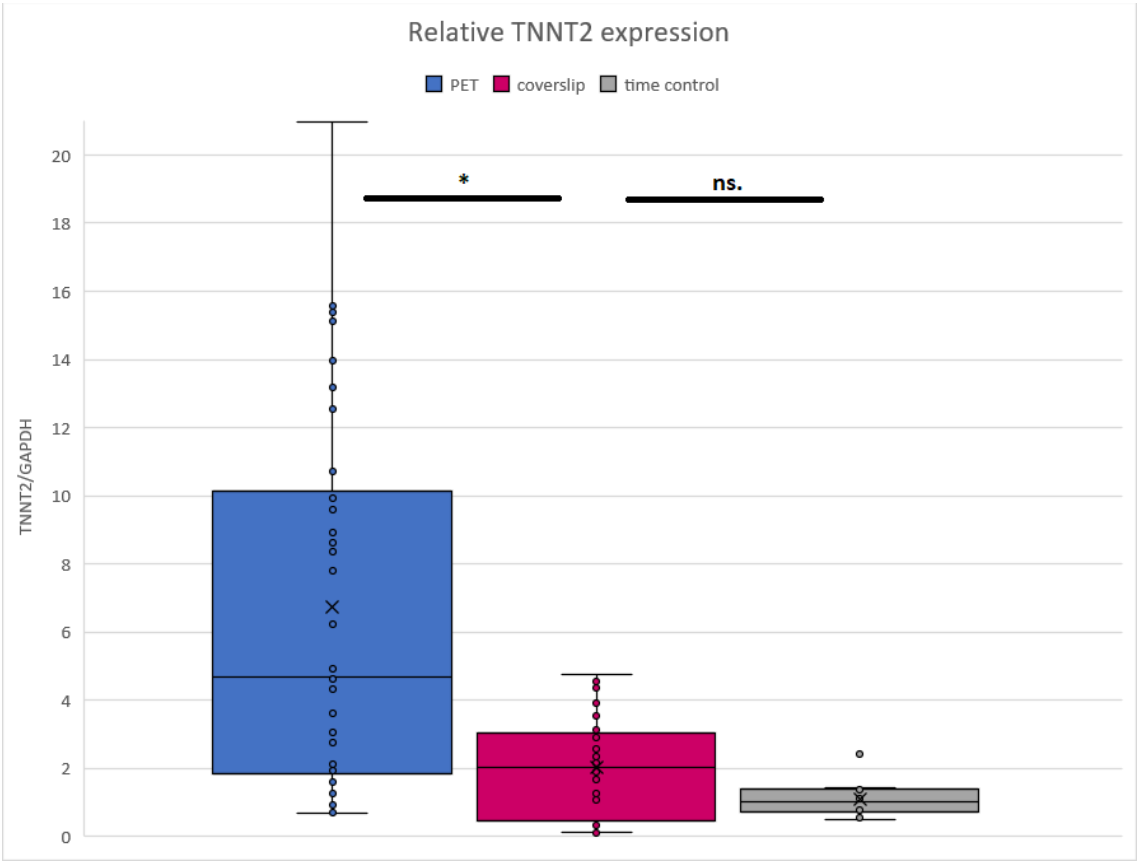

Figure 5. 4 *Relative TNNT2 expression of hiPSC-CMs grown on PET textiles and coverslips for 11 days and hiPSC-CMs grown on coverslips for 1 day (time control). The expressions are normalized to GAPDH.*

The difference in the average relative TNNT2 expression between hiPSC-CMs grown on PET textiles and coverslips for 11 days was statistically significant with 95 % certainty. The relative TNNT2 expression was 6.752 with 5.438 standard deviation for hiPSC-CMs grown on PET textiles and 2.014 with standard deviation of 1.391 for hiPSC-CMs grown on coverslips. Calculated from the averages, TNNT2 expression of the PET samples was approximately 3.35-fold greater than that of the coverslip samples.

The difference in the average relative TNNT2 expression between hiPSC-CMs grown on PET textiles for 11 days and time control was also statistically significant with 95 % certainty. The relative TNNT2 expression was 1.107 with 0.544 standard deviation for hiPSC-CMs grown on coverslips for 1 day. Thus, the TNNT2 expression of the PET samples was approximately 6.10-fold greater compared to the time control. On the other hand, the difference in TNNT2 expressions between hiPSC-CMs grown on coverslips for 11 days and 1 day was not statistically significant according to the two-tailed Mann-Whitney U test, even though when calculated from the averages, the TNNT2 expression increased 1.82-fold during the 11 days culture time. Here, higher number of time control samples would be required to reliably relate the significance of the results.

5.3 Calcium handling properties

Calcium imaging was performed to evaluate the functionality of hiPSC-CMs grown on PET textiles compared to hiPSC-CMs grown on coverslips. Cell permeable fluo-4 AM was used as labeled calcium indicator in the experiment. Adrenaline response of hiPSC-CMs grown on PET textiles was also tested. The cells were categorized as normal or abnormal based on the calcium transient profiles and abnormalities further into several groups. Statistical analysis was performed only to cells exhibiting normal calcium kinetics. Table 5.3 presents the percentage of normal hiPSC-CMs and cells exhibiting different abnormalities in the calcium handling properties. The abnormal peak shape in the table includes low/middle peaks and plateau abnormality. Figure 5.5 presents the normal peak shape and different abnormalities found in the calcium kinetics. The representative graphs can be from either PET samples or coverslip samples.

The 69.6 % of hiPSC-CMs grown on PET textiles exhibited normal calcium kinetics, while the amount was only 55.5 % for hiPSC-CMs grown on coverslips. The amount of plateau abnormality and low/middle peaks decreased from 30.6 % for hiPSC-CMs grown on coverslips to 17.4 % for hiPSC-CMs grown on PET textiles. The amounts of oscillations, double peaks and amplitude alterations were relatively small with small differences between the groups, and were 3.9 %, 3.5 % and 5.6 % for hiPSC-CMs grown on PET textiles and 2.8 %, 4.2 % and 6.9 % for hiPSC-CMs grown on coverslips, respectively.

Table 5. 3 *The percentage of cells exhibiting normal calcium kinetics and different abnormalities.*

Sample	Normal	Abnormal peak shape	Oscillation	Double peak	Amplitude alterations	Number of cells
PET	69.6 %	17.4 %	3.9 %	3.5 %	5.6 %	230
Coverslip	55.5 %	30.6 %	2.8 %	4.2 %	6.9 %	72

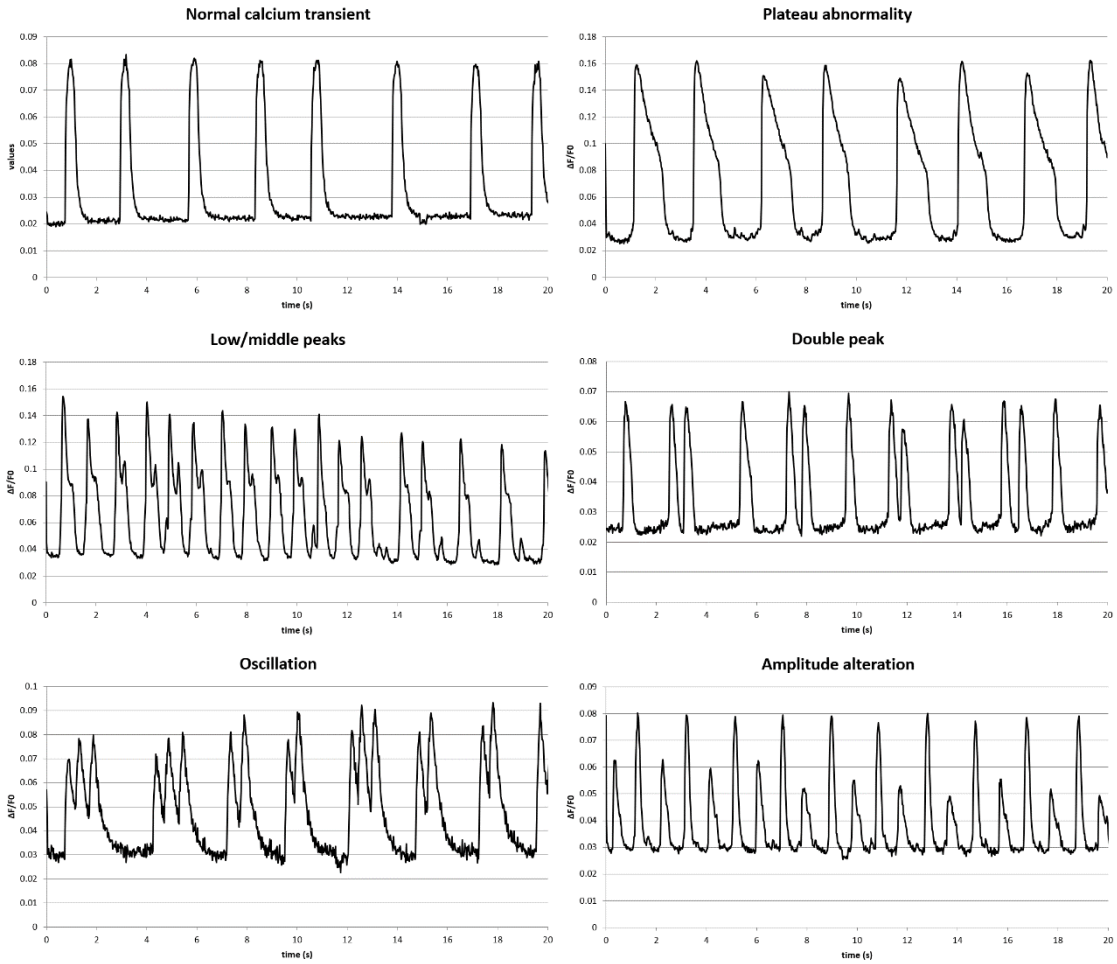

Figure 5. 5 *Normal calcium peak shape and different abnormalities in calcium kinetics. In plateau abnormality, the decay time of intracellular calcium is increased. In low/middle peak abnormality, the decreasing intracellular calcium starts to increase before lowering to the baseline. In oscillation abnormality, the cell cannot fully relax before a new contraction starts. In amplitude alteration, periodic changes occur in calcium peak amplitude and possibly in peak shape.*

The response of the hiPSC-CMs to adrenaline was also tested and recorded from 43 cells. 72 % of the cells clearly responded to adrenaline, while the response of 28 % of the cells was either unclear or did not occur. The most common response was increase in peak frequency indicating faster beating rate. Other responses included decrease in the amount of missing peaks or better beating rhythm indicated by more constant peak frequency. Sometimes after baseline measurement, the cells stopped beating, but started beating again after introducing adrenaline to the cells. This cannot be seen by comparing the baseline to the adrenaline measurement, so some cells that did respond to the adrenaline by starting to beat again, are not necessarily counted in the cells responding to adrenaline. Figure 5.6 shows different kinds of hiPSC-CM responses to adrenaline.

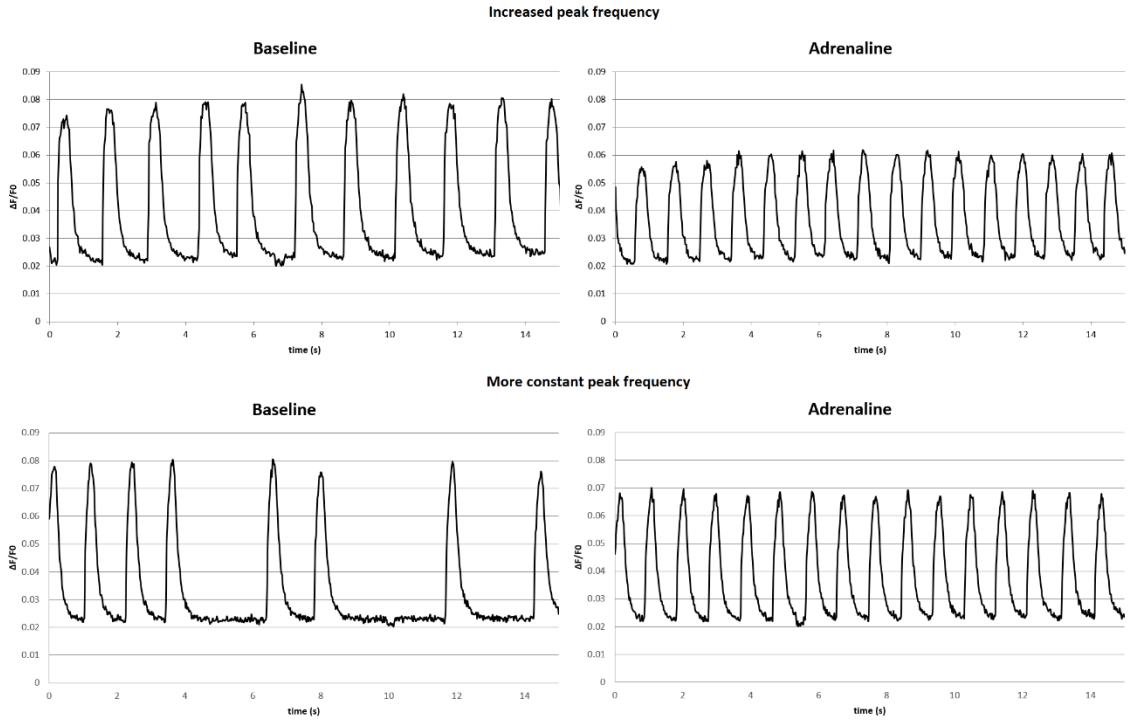

Figure 5. 6 *Adrenaline responses of hiPSC-CMs. The most common response was increase in peak frequency indicating of faster beating rate. Other common responses included more constant peak frequency and decrease in the number of missing peaks.*

Peak duration, rise time from 10 % to 90 %, decay time from 90 % to 10 % and peak frequency were determined from the data matrix derived from the calcium imaging video data to detect the differences in calcium handling properties of hiPSC-CMs cultured on PET textiles and coverslips exhibiting normal calcium transients. Table 5.4 presents the average values and standard deviations of peak duration, rise time, decay time and peak frequency of hiPSC-CMs grown on coverslips and PET textiles exhibiting normal calcium peaks. The results are further illustrated in figure 5.7.

Table 5. 4 *Average values and standard deviations of peak duration, rise time from 10 % to 90 %, decay time from 90 % to 10 % and peak frequency of hiPSC-CMs grown on PET textiles and coverslips.*

Sample	Peak duration (ms)	Rise time 10% to 90% (ms)	Decay time 90% to 10% (ms)	Peak frequency (Hz)
PET	582 ± 229	112 ± 49	295 ± 131	0.93 ± 0.52
coverslip	590 ± 202	90 ± 41	324 ± 96	0.75 ± 0.34

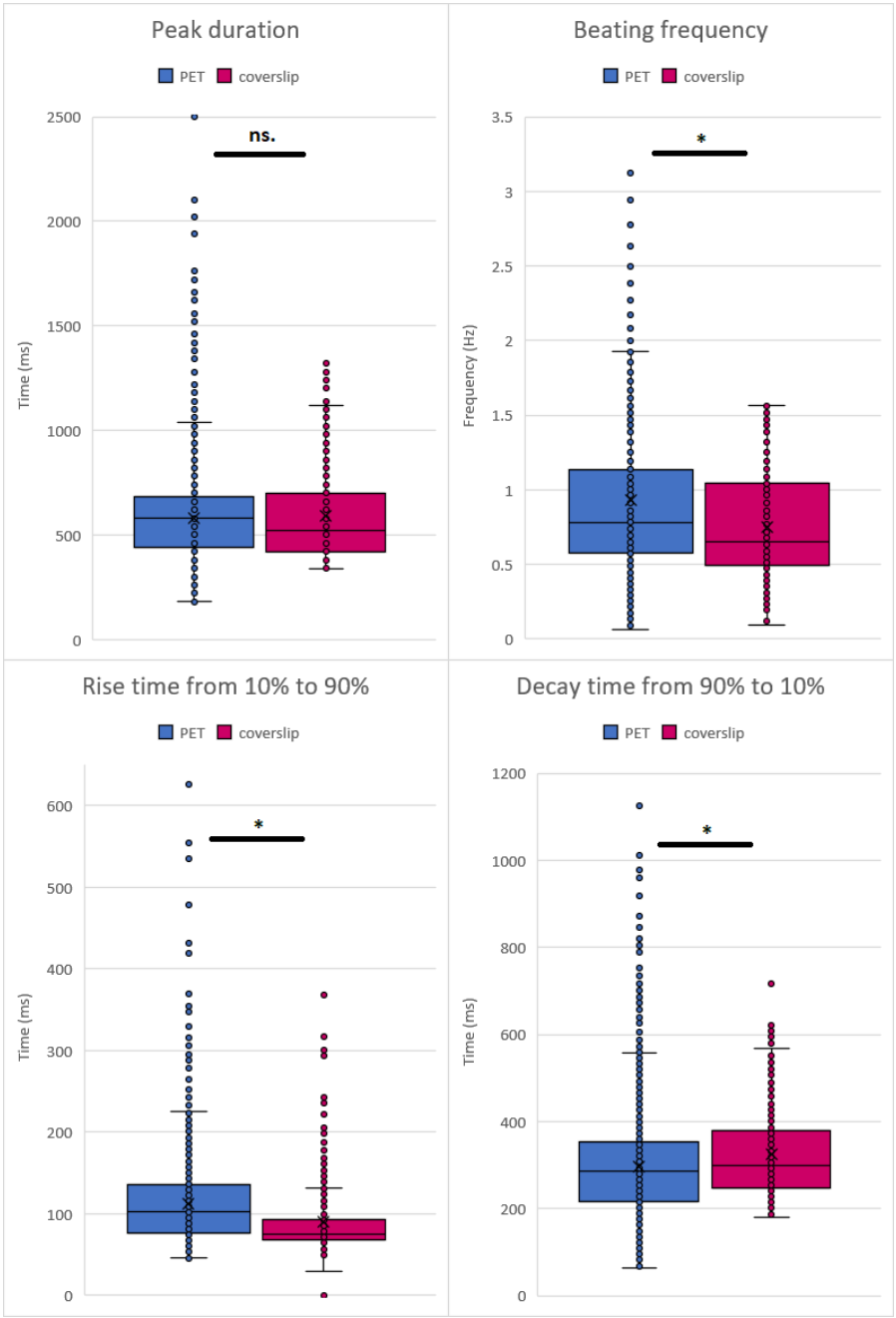

Figure 5. *7 Peak duration, rise time from 10 % to 90 %, decay time from 90 % to 10 % and beating frequency of hiPSC-CMs grown on PET textiles and coverslips exhibiting normal calcium kinetics.*

The difference in peak duration between PET and coverslips samples was not statistically significant. The average peak duration was 582 ms with 229 ms standard deviation for hiPSC-CMs grown on PET textiles and 590 ms with 202 ms standard deviation for hiPSC-CMs grown on coverslips. The difference is negligible with the large standard deviations. On the other hand, there was a statistically significant difference in rise time from 10 % to 90 % and in decay time from 90 % to 10 % between hiPSC-CMs grown on PET textiles and coverslips.

hiPSC-CMs grown on PET textiles had slower rise time but faster decay time compared to those grown on coverslips. The average rise time was 112 ms with 49 ms standard deviation for PET samples and 90 ms with 41 ms standard deviation for coverslips samples while the average decay time was 295 ms with 131 ms standard deviation for PET samples and 324 ms with 96 ms standard deviation for coverslip samples. There was also a statistically significant difference in peak frequency between hiPSC-CMs grown on PET textiles and coverslips with 95 % certainty. The average peak frequency was 0.93 Hz with 0.52 Hz standard deviation for PET samples and 0.75 Hz with 0.34 Hz standard deviation for coverslip samples.

6. DISCUSSION

In previous studies (Junnila 2016; Mansikkala 2017), our group determined that PET textiles can be used to improve structural maturation of hiPSC-CMs. However, structural properties are only one indicator of the maturation state of the cells and as such, they are not enough to confirm the effectiveness of the method in inducing the maturation of hiPSC-CMs. Thus, this study considered molecular and functional maturation state of the cells via qPCR and calcium imaging, respectively, along with structural properties via fluorescence staining and imaging.

6.1 Structural maturation

Structural properties were used as a maturation marker for hiPSC-CMs, since they are illustrative, and the morphology of the cells is important regarding their function. Three parameters were evaluated in this study. Circular variance from 0 to 1 describes the anisotropic alignment of the sarcomeres, zero meaning perfect anisotropic alignment and one meaning that the sarcomeres are not clearly aligned into any one direction. Modal sarcomere length describes the most common sarcomere length of the cell sarcomeres. Length to width ratio describes how longitudinally aligned the cell is, indicating of the rod-like shape of the cells.

The mean circular variance of the hiPSC-CMs grown on PET textiles was 0.611 and was lower than 0.882 of hiPSC-CMs grown on coverslips. The results were statistically significant and are in consensus with the results of the previous studies made by our group, where the circular variances of cells grown on textiles are lower compared to those of the cells grown on flat surfaces. However, the values differ a lot, as in the first study conducted by Junnila, the average circular variance for PET samples was 0.15 and for coverslip samples 0.40 (Junnila 2016) and in the second study by Mansikkala, the average circular variance for textile samples ranged from 0.22 to 0.46 depending on the textile type and coating and for coverslip samples the range was from 0.62 to 0.71 depending on the coating (Mansikkala 2017). The great differences in the results could be due to different differentiation protocol and addition of cell sorting step before plating the hiPSC-CMs on the textiles and coverslips.

Improved anisotropic sarcomere orientation was also observed in a study by Parrag *et al.*, where murine embryonic stem cell-derived cardiomyocytes were cultured on electrospun polyurethane aligned fiber scaffolds. The cells exhibited more organized sarcomere structures with cross-striations perpendicular to the major cell axis (Parrag, Zandstra & Woodhouse 2012). Furthermore, Han *et al.* reported more organized sarcomere structure on hiPSC-CMs cultured on aligned electrospun fiber scaffolds as did Rao *et al.* for hiPSC-

CMs cultured on microgrooved substrates (Han et al. 2016; Rao et al. 2013). These studies with our results indicates, that culturing PSC-derived cardiomyocytes on substrates providing structural guidance induces sarcomere orientation of the cells.

The difference modal sarcomere lengths of the hiPSC-CMs grown on PET textiles and coverslips was not statistically significant and was approximately 1.75 µm for both groups. Unlike in most other studied parameters, here, the standard deviations in both groups were relatively low and the results were more consistent. However, this only indicates that culturing the cells on PET textiles does not affect their sarcomere length, which is still significantly lower than 2.2 µm of adult CMs. The acquired results are in consensus with the results from the previous studies by our group, where the average modal sarcomere lengths varied approximately from 1.6 µm to 1.9 µm (Junnila 2016; Mansikkala 2017).

Compared to the study conducted by Han *et al.* where hiPSC-CMs were cultured on electrospun aligned fiber scaffolds, the sarcomere lengths they determined were significantly lower, only 1.4 µm on average. Similarly, they noticed no difference between the test and control groups (Han et al. 2016). As for Khan *et al.*, who cultured hiPSC-CMs on aligned nanofiber patches and flat culture plates, the sarcomere length increased from 1.59 µm to 1.68 µm with the cells cultured on nanofibers (Khan et al. 2015). Huethorst *et al.* cultured hiPSC-CMs on dual microgradient substrate and determined sarcomere length was 1.8 µm (Huethorst et al. 2016), which is close to results acquired in this study.

Furthermore, Wanjare *et al.* observed increase from 1.3 µm to 1.6 µm in hiPSC-CM sarcomere length when they compared cells cultured on aligned microfibrous PCL scaffolds and randomly oriented microfibrous scaffolds (Wanjare et al. 2017). As can be seen based on this and other studies made by our group (Junnila 2016; Mansikkala 2017) as well as studies made by other groups (Han et al. 2016; Huethorst et al. 2016; Khan et al. 2015), the sarcomere length of hiPSC-CMs vary relatively much but it seems that maturation methods based on topographical guidance of the cells cannot induce increase in sarcomere lengths to those observed in adult CMs.

Length to width ratio of hiPSC-CMs grown on PET textiles was statistically significantly greater compared to that of the cells of the coverslip samples. This indicates of more elongated morphology, which could be seen already from the images taken of the cells. As nothing guides the alignment of the hiPSC-CMs on flat coverslip substrates, the cells become round or polygonal and exhibit no clear longitudinal axis and had average length to width ratio of 1.6. On the other hand, when the hiPSC-CMs are cultured on PET textiles, they align and elongate according to the fibers and exhibit clear longitudinal axis. The average length to width ratio of PET samples was 4.9, which is much closer to 5-9 determined for adult CMs (Denning et al. 2016). Improvements in hiPSC-CM shape, including better cell alignment and elongation have been observed in multiple studies, where the hiPSC-CMs have been cultured on substrates providing structural guidance

(Han et al. 2016; Huethorst et al. 2016; Martella et al. 2017; Rao et al. 2013; Wanjare et al. 2017; Xu et al. 2017). Our results support these studies, indicating that culturing hiPSC-CMs on aligned fiber substrates improves the morphology of the cells.

There is some bias in the results regarding length to width ratio due to several reasons. The hiPSC-CMs grown on PET textiles can be partially under or in between the fibers, so determining accurately where the cell starts or ends was difficult in some cases. Also, the cells are flat against the fiber and can wrap around it, which can make them seem more rod-like in the images than they are. The autofluorescence from the PET textiles made it sometimes difficult to see the Troponin T staining used to determine cell borders, since they fluoresced on approximately same wavelength. Furthermore, with both hiPSC-CMs grown on PET textiles and coverslips, determining the border of two adjacent cells was difficult in some cases. Still, the difference in the length to width ratio of the two groups is so large, that we can be sure it is also due to the cell elongation.

One thing affecting the cell spreading and alignment is cell density. hiPSC-CMs grew sparsely on PET textiles, probably due to problems with the cell attachment to the textile structure. This can affect the structural properties, since the cells on coverslips did not have as much space to spread compared to cells on PET textiles. This can be seen in figure 5.1h, where the larger cell in the middle has had more space to spread compared to neighboring cells exhibits better sarcomere alignment and greater area. The cell is still more round than those grown on PET textiles. On the other hand, in figure 5.1e, the hiPSC-CMs grow more closely to each other and still exhibit clear sarcomere alignment and cell elongation according to the fibers. This indicates that also with higher cell density, the cells and their sarcomeres would align according to the fibers.

PET textiles and glass coverslips used in this study are both relatively stiff culture substrates. This can affect the structural properties, as was stated in a study by Herron *et al.* (2016). Herron *et al.* noticed that culturing hiPSC-CMs on Matrigel-coated soft PDMS substrates improved the structural properties of the cells, as well as gene expression and functionality of the cells. The culture substrate promoted intracellular gap junction formation, and inward rectifier potassium and sodium inward current densities were increased, which indicates of improved electrophysiological maturation. Furthermore, expression of integrin β1α5 receptor was increased. (Herron et al. 2016)

Based on this study as well as the previous studies made by our group (Junnila 2016; Mansikkala 2017), it seems that culturing hiPSC-CMs on PET textiles improves the cell shape, elongation and sarcomere orientation, but fails to affect the sarcomere length. As for the future, it would be interesting to further investigate the structural properties, for example T-tubule and M-line formation, since these structures are characteristic to cardiomyocytes but not seen in hiPSC-CMs and to our knowledge, any maturation method has not been able to induce their formation.

6.2 Relative gene expression

TNNT2 expression was chosen as a maturation marker for hiPSC-CMs, since it is a cardiac specific gene encoding cardiac muscle troponin T and it has been shown to be expressed lower levels in hiPSC-CMs compared to adult human CMs (Rao et al. 2013). The relative TNNT2 expression in hiPSC-CMs grown on PET textiles for 11 days was 3.35-fold on average compared to that of hiPSC-CMs grown on coverslips for 11 days. Compared to the time control, hiPSC-CMs cultured on coverslips for 1 day, the PET samples exhibited 6.10-fold increase in relative TNNT2 expression, on average.

TNNT2 was expressed higher levels in hiPSC-CMs grown on PET textiles compared to hiPSC-CMs grown on coverslips, which would suggest that the culture substrate influences the maturation state of the cells and that PET textiles would induce the maturation of the cells. This supports the results of the previous studies by our group, as well as this study, that culturing hiPSC-CMs on PET textiles could be used to induce the maturation of the cells as the structural properties of the hiPSC-CMs were improved compared to the control cells (Junnila 2016; Mansikkala 2017).

Both Han *et al.* as well as Wanjare *et al.* detected significantly higher TNNT2 expression levels when they cultured hPSC-CMs on electrospun aligned fibrous scaffolds compared and anisotropic microfibrous PCL scaffold compared to control cells cultured on flat surfaces or randomly aligned microfibrous PCL scaffolds (Han et al. 2016; Wanjare et al. 2017). These results are similar to what we observed in this study indicating that the maturation methods based on structural guiding of the cells could be effective in inducing both structural and molecular maturation of the hiPSC-CMs.

On the other hand, a similar cell aligning method, where the hiPSC-CM were cultured on microgrooved substrate, the structural properties of the cells were improved with alignment of the cells according to the grooves, but the molecular maturation or TNNT2 expression of the cells did not improve compared to control cells cultured on a flat surface. They included many structural genes and genes affecting calcium handling properties of the CMs to the study, but concluded that there were no meaningful differences in the expression levels of these genes even though some differences could be seen. (Rao et al. 2013)

The results could be different due to the culture and differentiation methods, or the time the hiPSC-CMs were cultured on the substrates providing topographical cues. However, it could also be that there is something in the aligned fiber structure or how the cells align according to them, that induces the molecular maturation of the cells, since now at least three studies have shown that aligned fibrous scaffolds are able to increase the expression of TNNT2 in hiPSC-CMs.

Also, hiPSC-CMs grown on coverslips for 11 days exhibited average 1.82-fold increase in TNNT2 expression compared to the time control, but this result was not statistically significant. However, figure 5.4 shows that even though the TNNT2 expression levels of the 11-day coverslip samples include more variation, higher number of the results are ranked above the time control results, indicating that with higher number of time control samples, the result might be significant. This would be in consensus with the results by Lundy *et al.*, who deduced that hiPSC-CMs cultured for longer periods exhibit more mature phenotype compared to hiPSC-CMs cultured for shorter periods, even though they did not use TNNT2 as a maturation marker (Lundy et al. 2013).

Based on these results, it seems that culturing hiPSC-CMs on PET textiles as well as longer culture time induces molecular maturation of the cells. In the future, the expression of multiple genes should be evaluated, as to get a comprehensive understanding about the effects of culturing hiPSC-CMs on PET textiles on their molecular maturation and gene expression. For example, Bedada *et al.* suggest that antithetically during fetal to adult type transition expressed TNNI2 and TNNI3 could be used as cardiomyocyte maturation markers as they are not susceptible to stress and not altered by disease conditions (Bedada, Wheelwright & Metzger 2016). The ratio they are expressed in, would indicate of the maturation state of the cells. Furthermore, expression of cardiac characteristic ion channel encoding genes, structural protein encoding genes as well as calcium cycling related genes, could be studied to get a proper idea of the maturation state of the hiPSC-CMs.

6.3 Calcium handling properties

Calcium handling properties of the hiPSC-CMs were studied by calcium imaging. Calcium cycling is an important factor in cardiomyocyte functionality, as it plays an important role in excitation contraction coupling (Ross & Pawlina 2016, pp. 334-335). The calcium kinetics of the hiPSC-CMs were classified as normal or abnormal based on the peak shape. The parameters of calcium kinetics chosen for closer inspection included peak duration, rise time from 10 % to 90 %, decay time from 90 % to 10 % and beating frequency, which were evaluated from the normal cells.

The percentage of hiPSC-CMs having normal calcium transients was larger in the PET samples compared to coverslip samples. It seemed that the culturing of the hiPSC-CMs on PET textiles decreased the number of cells exhibiting abnormal peak shape, including plateau abnormality and low/middle peaks, while the percentage of other abnormalities remained relatively unchanged, and were low per se. This alone could indicate that culturing the hiPSC-CMs on PET textiles improves calcium handling properties of the cells. On the other hand, as a wild type cell line, the cells should not exhibit as much abnormalities as these cells did. This could be due to variation in differentiation batches.

There was no statistically significant difference in peak duration between hiPSC-CMs cultured on PET textiles or coverslips. On the other hand, statistically significant differences in rise time from 10 % to 90 % and decay time from 90 % to 10 % were observed. Rise time from 10 % to 90 % was longer while decay time from 90 % to 10 % was shorter in hiPSC-CMs cultured on PET textiles compared to hiPSC-CMs grown on coverslips. Although, the sampling rate used in this study was 20 ms, so the results should be interpreted with precaution. The increase in rise time indicates that the release of calcium takes longer in hiPSC-CMs grown on PET textiles than in hiPSC-CMs grown on coverslips.

The shorter decay time indicates more efficient calcium removal from the cytoplasm. This could be due to enhanced calcium removal to outside of the cell via Na^{+}-Ca^{2+} exchanger or uptake to sarcoplasmic reticulum via sarco-endoplasmic reticulum calcium ATPase (Woodcock & Matkovich 2005). Also, activity of a protein encoded by phospholamban gene could be a reason behind the observed phenomenon, as it inhibits the activity of SERCA removing calcium from the cytosol (National Center for Biotechnology Information). The decrease in decay time can be affected by the adrenaline, since the adrenaline response of only hiPSC-CMs cultured on PET textiles was tested. Still, adrenaline was always washed out from the cells before new baseline measurements, but if the wash has not been sufficient for some reason, this can affect the results.

In turn, the longer rise time can be due to multiple reasons related to release of calcium ions either through the cell membrane or the sarcoplasmic reticulum, but it would require further investigation to determine the actual cause. For example, the possible lack of T-tubules, inefficient cell membrane polarization or differences in voltage-gated L-type calcium channels could cause the prolonged event. Of these reasons, lack of T-tubules is not a probable cause, since most likely both hiPSC-CMs cultured on PET textiles and coverslips lack them, as no maturation method has yet been able to induce T-tubule formation. Another reason could be differences in organization of the SR around the myofibrils, since the decay time was shorter in hiPSC-CMs grown on PET textiles, and the organization of the SR would probably affect that, too. Calcium induced calcium release from SR is mediated by ryanodine receptors, so differences for example in the expression of RYR2 could cause the increased rise time in hiPSC-CMs grown on PET textiles.

Khan *et al.* and Xu *et al.* had similar results when they cultured hiPSC-CMs on nanofiber patches and onion epithelium-like micropatterned chips, respectively. Both groups observed no differences in rise times between the groups, but the decay time was decreased with the cells on substrates providing structural guidance compared to cells on flat substrates (Khan et al. 2015; Xu et al. 2017). In turn, Rao *et al.* cultured hiPSC-CMs on microgrooved substrate and noticed shorter rise time and longer decay time in the calcium transients of the structured cells compared to that of control cells cultured on flat substrate. They suggested that the shorter rise time could be due to changes in calcium

entry and trigger for CICR. On the other hand, calcium uptake mechanisms had not undergone such changes and thus did not show any improvements (Rao et al. 2013).

Han *et al.* observed longer rise and decay times when they compared the calcium transients of hiPSC-CMs cultured on electrospun aligned fibrous scaffolds and flat tissue culture plastics and determined that cell alignment has only a limited effect on hiPSC-CM maturation. Unlike in our study as well as in studies conducted by Khan *et al.* and Rao *et al.*, after culturing the cells on fibrous scaffolds Han *et al.* replated them onto a flat surface and cultured the cells there for a few days (Han et al. 2016). This could explain the differences between the studies.

Beating frequency of the hiPSC-CMs cultured on PET textiles was higher on average compared to that of hiPSC-CMs cultured on coverslips and the difference was statistically significant. The frequency distribution of the PET samples was overall more towards the higher frequencies compared to coverslip samples, as can be seen in figure 5.7. Cells grown on PET textiles had average beating frequency of 0.93 Hz, which is approximately 56 beats per. Cells grown on coverslips had average beating frequency of 0.75 Hz, which in turn is approximately 45 beats per minute. Here, adrenaline testing performed only to PET samples could have an effect on the beating rate of the cells if the washout of the adrenaline was not sufficient.

Xu *et al.* had results similar to this study regarding the beating rate of hiPSC-CMs cultured on an onion epithelium-like micropatterned chip. They observed higher beating frequencies in hiPSC-CMs cultured on the chip compared to control cells cultured on a flat surface. The rates on day 11 after plating to the substrates were on average 55 beats per minute and 45 beats per minute, respectively. The rates were lower on the following days, but the difference increased significantly. On the final measurement on day 22, the beating rate of hiPSC-CMs cultured on the chips was approximately 75 beats per minute, while the beating rate of the control cells remained in 45 beats per minute. (Xu et al. 2017)

On the other hand, Rao *et al.* observed no significant differences in the beating rates of spontaneously beating hiPSC-CMs cultured on microgrooved and flat substrates. The beating rates were 11.67 beats per minute and 12.43, respectively (Rao et al. 2013). Wanjare *et al.* for one, observed significant decrease in spontaneous beating of hiPSC-CMs grown on aligned microfibrous scaffolds compared to random microfibrous scaffolds. The beating frequency decreased from 27 beats per minute to 9 beats per minute (Wanjare et al. 2017). The beating rates observed in the studies by Rao *et al.* and Wanjare *et al.* are significantly lower compared to those observed in this study. This could be due to many reasons, including maturation state of the cells, cell density on the substrates, culture conditions, such as medium, pH and temperature. Also, the imaging conditions, such as temperature and pH changes, can affect the beating characteristics of the cells (Laurila et al. 2016).

As with the results from structural properties and gene expression, the standard deviations of the calcium imaging results are relatively large, which can be seen from figure 5.7. What is interesting, is that in all cases, including TNNT2 expression and structural properties, the distribution of the values of PET samples is much wider compared to that of coverslip samples. The variation in the results could be caused by the textile, if it affects the cells differently considering whether the cells have grown in isolation, between the fibers or on top of the fibers. The conditions are more stable in coverslip samples, which could result in less variation in the results.

Adrenaline response of hiPSC-CMs cultured on PET textiles was evaluated and the cells clearly responded to adrenaline. This was observed as an increase in beating frequency, decrease in missing peaks and as a more regular beating rate. Also, in some cases the cells that had stopped contracting, started to beat again after introducing adrenaline. This indicates that the hiPSC-CMs exhibit beta-adrenergic receptors and are able to respond to adrenaline as expected of cardiomyocytes.

A possible source of error regarding calcium imaging results is difference in cell density between the samples. In the first set of samples the cell density was lower compared to the second set of samples. Also, in the same set of samples, the coverslip samples had higher cell density than the PET samples, since the cells do not attach that well on the PET textiles and probably slide through the textile fibers, which leads to lower cell density. Cell density affects the calcium transients, because if the cells are in contact with each other, they contract synchronously, and different abnormalities are not visible that easily. Thus, it is possible that the improved calcium uptake, higher beating frequency and decrease in abnormalities are partially due to the higher cell density in the second set of samples. Still, it seems that the calcium handling properties of the hiPSC-CMs cultured on PET textiles were improved compared to that of hiPSC-CMs cultured on coverslips.

As for the future, it would be interesting to further investigate where the differences in rise and decay times between hiPSC-CMs cultured on PET textiles and coverslips arise. Furthermore, the differentiation method and magnetic activated cell sorting seem to affect the calcium handling properties of the cells, which would be essential to prove. Also, whether the change from Matrigel to gelatin as a coating material during cell passaging affects the calcium handling properties of the cells should be investigated.

7. CONCLUSIONS

The aims of this study were to discover whether culturing hiPSC-CMs on PET textiles affects molecular maturation and functionality of the cells in addition to structural properties. Molecular maturation was studied by comparing TNNT2 expression of hiPSC-CMs cultured on PET textiles to that of hiPSC-CMs cultured on flat coverslips. Functionality of the cells was assessed via calcium imaging. Also, structural properties were further evaluated by immunofluorescence staining and fluorescence imaging. The studied structural properties included sarcomere orientation and length and cell shape.

The relative TNNT2 expression was higher in hiPSC-CMs cultured on PET textiles compared to that of hiPSC-CMs cultured on coverslips. The increase was clear and indicates that hiPSC-CMs cultured on PET textiles have improved maturation state compared to the control. Also, the calcium kinetics of hiPSC-CMs cultured on PET textiles seemed to improve. The number of cells exhibiting abnormal peak shape decreased and the cells showed improved calcium removal from the cytoplasm. On the other hand, the release of calcium into the cytoplasm was slightly slower in hiPSC-CMs cultured on PET textiles. hiPSC-CMs cultured on PET textiles exhibited better structural properties, including increased sarcomere orientation as well as elongated cell shape. Then again, there were no differences in sarcomere length, which is significantly lower in both groups compared to that observed in adult CMs.

Altogether, culturing hiPSC-CMs on PET textiles seems to induce both molecular and structural maturation as well as functionality of the cells, while the cells still show signs of immature phenotype. Also, further investigation should be done regarding expression of other genes characteristic to mature CMs as well as reasons for changes in calcium kinetics of the hiPSC-CMs grown on PET textiles. As for the structural properties, T-tubule formation as well as organization of the sarcoplasmic reticulum could provide further insights to the maturation state of the cells.

REFERENCES

Almeida, M., García-Montero, A.C. & Orfao, A. (2014). Cell purification: A new challenge for biobanks, Pathobiology, Vol. 81, pp. 261–275.

Bedada, F.B., Wheelwright, M. & Metzger, J.M. (2016). Maturation status of sarcomere structure and function in human iPSC-derived cardiac myocytes, Biochimica et Biophysica Acta - Molecular Cell Research, Vol. 1863, No. 7, pp. 1829–1838.

Benton, G., Arnaoutova, I., George, J., Kleinman, H.K. & Koblinski, J. (2014). Matrigel: From discovery and ECM mimicry to assays and models for cancer research, Advanced Drug Delivery Reviews, Vol. 79-80, pp. 3–18.

Bigelow, C.E. (2005). Biological Applications of Confocal Fluorescence Polarization Microscopy, Master's Thesis, University of Rochester, The Institute of Optics, Rochester, p. 165. Available: https://www.urmc.rochester.edu/MediaLibraries/URMCMedia/labs/foster-lab/documents/bigelow-thesis.pdf

Burridge, P.W., Thompson, S., Millrod, M.A., Weinberg, S., Yuan, X., Peters, A., Mahairaki, V., Koliatsos, V.E., Tung, L. & Zambidis, E.T. (2011). A Universal System for Highly Efficient Cardiac Differentiation of Human Induced Pluripotent Stem Cells That Eliminates Interline Variability, PLoS ONE, Vol. 6, No. 4.

Burridge, P.W., Holmström, A. & Wu, J.C. (2015). Chemically Defined Culture and Cardiomyocyte Differentiation of Human Pluripotent Stem Cells. In: *Current Protocols in Human Genetics*. pp. 21.3.1–21.3.15.

Carson, D., Hnilova, M., Yang, X., Nemeth, C.L., Tsui, J.H., Smith, A.S.T., Jiao, A., Regnier, M. Murry, C.E., Tamerler, C. & Kim, D.H. (2016). Nanotopography-Induced Structural Anisotropy and Sarcomere Development in Human Cardiomyocytes Derived from Induced Pluripotent Stem Cells, ACS Applied Materials and Interfaces, Vol. 8, No. 34, pp. 21923–21932.

Chun, Y.W., Balikov, D.A., Feaster, T.K., Williams, C.H., Sheng, C.C., Lee, J.-B., Boire, T.C., Neely, M.D., Bellan, L.M., Ess, K.C., Bowman, A.B., Sung, H.-J. & Hong, C.C. (2015). Combinatorial polymer matrices enhance in vitro maturation of human induced pluripotent stem cell-derived cardiomyocytes, Biomaterials, Vol. 67, pp. 52–64.

Daley, G.Q. (2015). Stem cells and the evolving notion of cellular identity, Philosophical transactions of the Royal Society of London. Series B, Biological sciences, Vol. 370, No. 1680.

Denning, C., Borgdorff, V., Crutchley, J., Firth, K.S.A, George, V., Kalra, S., Kondrashov, A., Hoang, M.D., Mosqueira, D., Patel, A., Prodanov, L., Rajamohan, D.,

Skarnes, W., Smith, J.G.W. & Young, L.E. (2016). Cardiomyocytes from human pluripotent stem cells: From laboratory curiosity to industrial biomedical platform, Biochimica et Biophysica Acta - Molecular Cell Research, Vol. 1863, No. 7, pp. 1728–1748.

Di Pasquale, E., Song, B. & Condorelli, G. (2013). Generation of Human Cardiomyocytes: A Differentiation Protocol from Feeder- free Human Induced Pluripotent Stem Cells, Journal of Visualized Experiments, Vol. 50429, No. 7610, pp. 1–6.

Donaldson, J.G. (2015). Immunofluorescence Staining, in: Bonifacino, J.S., Harford, J.B., Lippincott-Schwartz, J. & Yamada, K.M. (ed.), Current Protocols in Cell Biology, Vol. 69, John Wiley & Sons, Inc., Hoboken, USA, pp. 4.3.1–4.3.7.

Dulak, J., Szade, K., Szade, A., Nowak, W. & Józkowicz, A. (2015). Adult stem cells: hopes and hypes of regenerative medicine* Acta Biochimica Polonica, Vol 62, No. 3, pp. 329–337.

Feaster, T.K., Cadar, A.G., Wang, L., Williams, C.H., Chun, Y.W., Hempel, J.E., Bloodworth, N., Merryman, W.D., Lim, C.C., Wu, J.C., Knollmann, B.C. & Hong, C.C. (2015). Matrigel Mattress: A Method for the Generation of Single Contracting Human-Induced Pluripotent Stem Cell-Derived Cardiomyocytes, Circulation Research, Vol. 117, No. 12.

Gee, K.R., Brown, K.A., Chen, W.-N. U., Bishop-Stewart, J., Gray, D. & Johnson, I. (2000). Chemical and physiological characterization of fluo-4 Ca^{2+} -indicator dyes, Cell Calcium, Vol. 27, No. 2, pp. 97–106.

Golob, M., Moss, R.L. & Chelser, N.C. (2014). Cardiac Tissue Structure, Properties, and Performance: A Materials Science Perspective, Annals of Biomedical Engineering, Vol. 42, No. 10, pp. 2986–3005.

Han, J., Wu, Q., Xia, Y., Wagner, M.B., Xu, C. (2016). Cell alignment induced by anisotropic electrospun fibrous scaffolds alone has limited effect on cardiomyocyte maturation, Stem Cell Research, Vol. 16, No. 3, pp. 740–750.

Herron, T.J., Da Rocha, A.M., Campbell, K., Ponce-Balbuena, D., Willis, B.C., Guerrero-Serna, G., Liu, Q., Klos, M., Musa, H., Zarzoso, M., Bizy, A., Furness, J., Anumonwo, J., Mironov, S. & Jalife, J. (2016). Extracellular Matrix Mediated Maturation of Human Pluripotent Stem Cell Derived Cardiac Monolayer Structure and Electrophysiological Function, Circulation: Arrhythmia and Electrophysiology, Vol. 9, No. 4.

Hirt, M.N., Hansen, A. & Eschenhagen, T. (2014). Cardiac tissue engineering: State of the art, Circulation Research, Vol. 114, No. 2, pp. 354–367.

Hossler, F.E. (2014). Ultrastructure atlas of human tissues, Wiley-Blackwell, New Jersey, p. 968.

Huethorst, E., Hortigon, M., Zamora-Rodriguez, V., Reynolds, P.M., Burton, F., Smith, G. & Gadegaard, N. (2016). Enhanced Human-Induced Pluripotent Stem Cell Derived Cardiomyocyte Maturation Using a Dual Microgradient Substrate, ACS Biomaterials Science and Engineering, Vol. 2, No. 12, pp. 2231–2239.

Hulett, H.R., Bonner, W.A., Barrett, J. & Herzenberg, L.A (1969). Cell Sorting: Automated Separation of Mammalian Cells as a Function of Intracellular Fluorescence, Science, Vol. 166, No. 3906, pp. 747–749.

Iseoka, H., Miyagawa, S., Fukushima, S., Saito, A., Masuda, S., Yajima, S., Ito, E., Sougawa, N., Takeda, M., Harada, A., Lee, J.-K. & Sawa, Y. (2017). Pivotal role of non-cardiomyocytes in electromechanical and therapeutic potential of induced pluripotent stem cell-derived engineered cardiac tissue, Tissue Engineering Part A.

Junnila, A. (2016). Human Induced Pluripotent Stem Cell Derived Cardiomyocytes Grown on Woven Polyethylene Terephthalate Textile, Master's Thesis, Tampere University of Technology, Faculty of Engineering Sciences, Tampere, p. 71. Available: http://URN.fi/URN:NBN:fi:tty-201605244038

Kalra, K. & Tomar, P. (2014). Stem Cell: Basics, Classification and Applications, American Journal of Phytomdicine and Clinical Therapeutics, Vol. 2, No. 7, pp. 919–930.

Karakikes, I., Senyei, G., Hansen, J., Kong, C.-W., Azeloglu, E.U., Stillitano, F., Lieu, D.K., Wang, J., Ren, L., Hulot, J.-S., Iyengar, R., Li, R.A. & Hajjar, R.J. (2014). Small molecule-mediated directed differentiation of human embryonic stem cells toward ventricular cardiomyocytes, Stem Cells Translational Medicine, Vol. 3, No. 1, pp. 18–31.

Karakikes, I., Ameen, M., Termglinchan, V. & Wu, J.C. (2015). Human Induced Pluripotent Stem Cell-Derived Cardiomyocytes: Insights into Molecular, Cellular, and Functional Phenotypes, Circulation Research, Vol. 117, No. 1, pp. 80–88.

Kartasalo, K., Pölönen, R.-P., Ojala, M., Rasku, J., Lekkala, J., Aalto-Setälä, K. & Kallio, P. (2015). CytoSpectre: a tool for spectral analysis of oriented structures on cellular and subcellular levels, BMC bioinformatics, Vol. 16, No. 344, pp. 1–23.

Katrukha, I.A. (2013). Human cardiac troponin complex. Structure and functions, Biochemistry. Biokhimiia, Vol. 78, No. 13, pp. 1447–1465.

Khan, M., Xu, Y., Hua, S. Johnson, J. Belevych, A., Janssen, P.M.L., Gyorke, S., Guan, J. & Angelos, M.G. (2015). Evaluation of changes in morphology and function of human induced pluripotent stem cell derived cardiomyocytes (hiPSC-CMs) cultured on an aligned-nanofiber cardiac patch, PLoS ONE, Vol. 10, No. 5.

Kreutzer, J., Ikonen, L., Hirvonen, J., Pekkanen-Mattila, M., Aalto-Setälä, K. & Kallio, P. (2014). Pneumatic cell stretching system for cardiac differentiation and culture, Medical Engineering and Physics, Vol. 36, pp. 496–501.

Laurila, E., Ahola, A., Hyttinen, J. & Aalto-Setälä, K. (2016). Methods for in vitro functional analysis of iPSC derived cardiomyocytes – Special focus on analyzing the mechanical beating behavior, Biochimica et Byíophysica Acta – Molecular Cell Research, Vol. 1863, pp. 1864–1872.

Lavrentovich, O. (2012). Confocal Fluorescence Microscopy, in: Kaufmann, E. N. (ed.), Characterization of Materials, John Wiley & Sons, Inc., New York, USA, pp. 1–15.

Leung, H.W., Moerkamp, A.T., Padmanabhan, J., Ng, S.-W., Goumans, M.-J. & Choo, A. (2015). mAb C19 targets a novel surface marker for the isolation of human cardiac progenitor cells from human heart tissue and differentiated hESCs, Journal of Molecular and Cellular Cardiology, Vol. 82, pp. 228–237.

Livak, K.J. & Schmittgen, T.D. (2001). Analysis of relative gene expression data using real-time quantitative PCR and 2-ΔΔCT method, Methods, Vol. 25, pp. 402–408.

Lundy, S.D., Zhu, W.-Z., Regnier, M. & Laflamme, M.A. (2013). Structural and functional maturation of cardiomyocytes derived from human pluripotent stem cells, Stem Cells and Development, Vol. 22, No. 14, pp. 1991–2002.

Ma, J., Guo, L., Fiene, S.J., Anson, B.D., Thomson, J.A., Kamp, T.J., Kolaja, K.L., Swanson, B.J. & January, C.T. (2011). High purity human-induced pluripotent stem cell-derived cardiomyocytes: electrophysiological properties of action potentials and ionic currents, Americal Journal of Physiology: Heart and Circulation Physiology, Vol. 301, No. 5, pp. 2006–2017

Mansikkala, L.T. (2017). Enhancing the Structural Maturation and Attachment of Human Induced Pluripotent Stem Cell Derived Cardiomyocytes on Textile Surfaces, Master's Thesis, Tampere University of Technology, Faculty of Natural Sciences, Tampere, p. 74. Available: http://URN.fi/URN:NBN:fi:tty-201703131159

Martella, D., Paoli, P., Pioner, J.M., Sacconi, L., Coppini, R., Santini, L., Lulli, M., Cerbai, E., Wiersma, D.S., Poggesi, C., Ferrantini, C. & Parmeggiani C. (2017) Liquid Crystalline Networks toward Regenerative Medicine and Tissue Repair, Small.

Masumoto, H., Nakane, T., Tinney, J.P., Yuan, F., Ye, F., Kowalski, W.J., Minakata, K., Sakata, R., Yamashita, J.K. & Keller, B.B. (2016). The myocardial regenerative potential of three-dimensional engineered cardiac tissues composed of multiple human iPS cell-derived cardiovascular cell lineages, Scientific Reports, Vol. 6, No. 1.

Miltenyi, S., Müller, W., Weichel, W. & Radbruch, A. (1990). High gradient magnetic cell separation with MACS., Cytometry, Vol. 11, No. 2, pp. 231–238.

Moreau, D., Stockslager, J.L., Cheli, R., Haworth, K. (2002). Anatomy & Physiology (2nd ed.), Lippincott Williams & Wilkins, Pennsylvania, p. 255.

Mueller, M. (2005). Introduction to Confocal Fluorescence Microscopy (2nd ed.), SPIE Press, Washington, USA, p. 121.

Mummery, C.L., Zhang, J., Ng, E.S., Elliot, D.A., Elefanty, A.G. & Kamp, T.J. (2012). Differentiation of human embryonic stem cells and induced pluripotent stem cells to cardiomyocytes: A methods overview, Circulation Research, Vol. 111, No. 3, pp. 344–358.

Narazaki, G., Uosaki, H., Teranishi, M., Okita, K., Kim, B., Matsuoka, S., Yamanaka, S. & Yamashita, J.K. (2008). Directed and systematic differentiation of cardiovascular cells from mouse induced pluripotent stem cells, Circulation, Vol. 8, No. 5, pp. 498–506.

National Center for Biotechnology Information [WWW]. [cited 21.11.2017]. Available at https://www.ncbi.nlm.nih.gov/gene/.

Neurauter, A.A., Bonyhadi, M., Lien, E., Nøkleby, L., Ruud, E., Camacho, S. & Aarvak, T. (2007). Cell isolation and expansion using dynabeads, in: Scheper T.H., Belkin, S., Bley, T.H., Bohlmann, J., Gu, M.B., Hu, W.-S., Mattiasson, B., Nielsen, J., Seitz, H., Ulber, R., Zeng, A.-P., Zhong, J.-J. & Zhou, W. (ed.), Advances in Biochemical Engineering/Biotechnology, Heidelberg: Springer Berlin Heidelberg, Berlin, pp. 41–73.

Nunes, S.S., Miklas, J.W., Liu, J., Aschar-Sobbi, R., Xiao, Y., Zhang, B., Jiang, J., Masse, S., Gagliardi, M., Hsieh, A., Thavandiran, N., Laflamme, M.A., Nanthakumar, K., Gross, G., Backx, P.H., Keller, G. & Radisic, M. (2013). Biowire: a platform for maturation of human pluripotent stem cell-derived cardiomyocytes, Nature Methods, Vol. 49, No. 2, pp. 781–787.

Oreopoulos, J., Berman, R. & Browne, M. (2014). Spinning disk confocal microscopy: present technology and future trends, in: Waters, J.C. & Wittman, T. (ed.), Quantitative Imaging in Cell Biology, Methods in Cell Biology, Vol. 123, Academic Press, pp. 153–175.

Paddock, S.W. & Eliceiri, K.W. (2014). Laser scanning confocal microscopy: History, applications, and related optical sectioning techniques., in Paddock, S.W. (ed.), Confocal Microscopy: Methods and Protocols (2nd ed.), Methods in Molecular Biology, Vol. 1075, Humana Press, Madison, USA, pp. 9–47.

Parrag, I.C., Zandstra, P.W. & Woodhouse, K.A. (2012). Fiber alignment and coculture with fibroblasts improves the differentiated phenotype of murine embryonic stem cell-derived cardiomyocytes for cardiac tissue engineering, Biotechnology and Bioengineering, Vol. 109, No. 3, pp. 813–822.

Price, R.L., Haley, S.T., Bullard, T., Davis, J., Borg, T.K. & Terracio, L. (2014). Confocal Microscopy of Cardiac Myocytes, in: Paddock, S.W. (ed.), Confocal Microscopy: Methods and Protocols (2nd ed.), Methods in Molecular Biology, Vol. 1075, Humana Press, Madison, USA, pp. 185–199.

Rao, C., Prodromakis, T., Kolker, L. Chaudhry, U.A.R., Trantidou, T., Sridhar, A.,

Weekes, C., Camelliti, P., Harding, S.E., Darzi, A., Yacoub, M.H., Athanasiou, T. & Terracciano, C.M. (2013). The effect of microgrooved culture substrates on calcium cycling of cardiac myocytes derived from human induced pluripotent stem cells, Biomaterials, Vol. 34, No. 10, pp. 2399–2411.

Robertson, C., Tran, D.D. & George, S.C. (2013). Concise review: maturation phases of human pluripotent stem cell-derived cardiomyocytes, Stem cells, Vol. 31, No. 5, pp. 829–837.

Ross, M.H. & Wojciech, P.I. (2016). Histology: A text and atlas, with correlated cell and molecular biology (7th ed.), Woltwrs Kluwer Health, Philadelphia, p. 992.

Ruan, J.L., Tulloch, N.L., Razumova, M.V., Saiget, M., Muskheli, V., Pabon, L., Reinecke, H., Regnier, M. & Murry, C.E. (2016). Mechanical Stress Conditioning and Electrical Stimulation Promote Contractility and Force Maturation of Induced Pluripotent Stem Cell-Derived Human Cardiac Tissue, Circulation, Vol. 134, No. 20, pp. 1557–1567.

Sarantitis, I., Papanastasopoulos, P., Manousi, M., Baikoussis, N.G. & Apostolakis, E. (2012). The cytoskeleton of the cardiac muscle cell, Hellenic Journal of Cardiology, Vol. 53, No. 5, pp. 367–379.

Schwach, V. & Passier, R. (2016). Generation and purification of human stem cell-derived cardiomyocytes, Differentiation, Vol. 91, No. 4–5, pp. 126–138.

Severs, N.J. (2000). The cardiac muscle cell, BioEssays, Vol. 22, No. 2, pp. 188–199.

Sharma, A., Li, G., Rajarajan, K., Hamaguchi, R., Burridge, P.W. & Wu, S.M. (2015). Derivation of highly purified cardiomyocytes from human induced pluripotent stem cells using small molecule-modulated differentiation and subsequent glucose starvation, Journal of visualized experiments: Journal of Visualized Experiments, No. 97.

Sheikh, F., Lyon, R.C. & Chen, J. (2015). Functions of Myosin Light Chain-2 (MYL2) in Cardiac Muscle and Disease, Gene, Vol. 569, No. 1, pp. 14–20.

Shields IV, C.W., Reyes, C.D. & López, G.P. (2015). Microfluidic cell sorting: a review of the advances in the separation of cells from debulking to rare cell isolation, Lab on a Chip, Vol. 15, No. 5, pp. 1230–1249.

Sjöblom, B., Salmazo, A. & Djinović-Carugo, K. (2008). α-actinin structure and regulation, Cellular and Molecular Life Sciences, Vol. 65, No. 17, pp. 2688–2701.

Smith, A.S.T., Macadangdang, J., Leung, W., Laflamme, M.A. & Kim, D.-H. (2017). Human iPSC-derived cardiomyocytes and tissue engineering strategies for disease modeling and drug screening, Biotechnology Advances, Vol. 35, No. 1, pp. 77–94.

Takahashi, K., Tanabe, K., Ohnuki, M., Narita, M., Ichisaka, T., Tomoda, K. &

Yamanaka, S. (2007). Induction of Pluripotent Stem Cells from Adult Human Fibroblasts by Defined Factors, Cell, Vol. 131, No. 5, pp. 861–872.

Takahashi, K. & Yamanaka, S. (2006). Induction of Pluripotent Stem Cells from Mouse Embryonic and Adult Fibroblast Cultures by Defined Factors, Cell, Vol. 126, No. 4, pp. 663–676.

Talkhabi, M., Aghdami, N. & Baharvand, H. (2016). Human cardiomyocyte generation from pluripotent stem cells: A state-of-art, Life Sciences, Vol. 145, pp. 98–113.

Tohyama, S., Hattori, F., Sano, M., Hishiki, T., Nagahata, Y., Matsuura, T., Hashimoto, H., Suzuki, T., Yamashita, H., Satoh, Y., Egashira, T., Seki, T., Muraoka, N., Yamakawa, H., Ohgino, Y., Tanaka, T., Yoichi, M., Yuasa, S., Murata, M., Suematsu, M. & Fukuda, K. (2013). Distinct Metabolic Flow Enables Large-Scale Purification of Mouse and Human Pluripotent Stem Cell-Derived Cardiomyocytes, Cell Stem Cell, Vol. 12, No. 1, pp. 127–137.

Tzatzalos, E, Abilez, O.J., Shukla, P. & Wu, J.C. (2016). Engineered heart tissues and induced pluripotent stem cells: Macro- and microstructures for disease modeling, drug screening, and translational studies, Advanced Drug Delivery Reviews, Vol. 96, pp. 234–244.

Van Dijk, S.J., Bezold, K.L. & Harris, S.P. (2014). Earning Stripes: Myosin Binding Protein-C Interactions with Actin, Pflugers Archiv European Journal of Physiology, Vol. 466, No. 3, pp. 445–450.

Veuthey, T., Herrera, M.G. & Dodero, V.I. (2014). Dyes and Stains: from molecular structure to histological application, Frontiers in Bioscience, Vol. 19, No. 1, pp. 91–112.

Vuorenpää, H., Penttinen, K., Heinonen, T., Pekkanen-Mattila, M., Sarkanen, J.-R., Ylikomi, T. & Aalto-Setälä, K. (2017). Maturation of human induced pluripotent stem cell derived cardiomyocytes is improved in cardiovascular construct, Cytotechnology, Vol. 69, pp. 785-800.

Wanjare, M., Hou, L., Nakayama, K.H., Kim, J.J., Mezak, N.P., Abilez, O.J., Tzatzalos, E., Wu, J.C. & Huang, N.F. (2017) Anisotropic microfibrous scaffolds enhance the organization and function of cardiomyocytes derived from induced pluripotent stem cells, Biomaterials Science, Vol. 5, No. 8, pp. 1567-1578.

Woodcock, E.A. & Matkovich, S.J. (2005). Cardiomyocytes structure, function and associated pathologies, International Journal of Biochemistry and Cell Biology, Vol. 37, No. 9, pp. 1746–1751.

World Health Organization (2017). Cardiovascular diseases (CVDs), web page. Avaliable (accessed 24.5.2017): http://www.who.int/mediacentre/factsheets/fs317/en/

Xu, C., Wang, L., Yu, Y., Yin, F., Zhang, X., Jiang, L. & Qin, J. (2017) Bioinspired onion epithelium-like structure promotes the maturation of cardiomyocytes derived from human pluripotent stem cells, Biomaterials Science, Vol. 5, No. 9, pp. 1810-1819.

Yang, X., Pabon, L. & Murry, C.E. (2014). Engineering adolescence: Maturation of human pluripotent stem cell-derived cardiomyocytes, Circulation Research, Vol. 114, No. 3, pp. 511–523.

Ye, L., Zhang, S., Greder, L., Dutton, J., Keirstead, S.A., Lepley, M., Zhang, L., Kaufman, D. & Zhang, J. (2013). Effective Cardiac Myocyte Differentiation of Human Induced Pluripotent Stem Cells Requires VEGF, PLoS ONE, Vol. 8, No. 1.

Yin, P.T., Han, E. & Lee, K.B. (2016). Engineering Stem Cells for Biomedical Applications, Advanced Healthcare Materials, Vol. 5, No. 1, pp. 10–55.